

2016

## Examining the Effect of Introducing a Link from Electrical Excitation to Calcium Dynamics in a Cardiomyocyte

Kallista Angeloff

University of Washington, angeloff@uw.edu

Carlos A. Barajas

Olivet College, cbarajas@olivetcollege.edu

Alexander Middleton

Winthrop University, middletona6@winthrop.edu

Uchenna Osia

University of Maryland, Baltimore County, osiau1@umbc.edu

Jonathan S. Graf

University of Maryland, Baltimore County, jongraf1@umbc.edu

*See next page for additional authors*

Follow this and additional works at: <https://ir.library.illinoisstate.edu/spora>

---

### Recommended Citation

Angeloff, Kallista; Barajas, Carlos A.; Middleton, Alexander; Osia, Uchenna; Graf, Jonathan S.; Gobbert, Matthias K.; and Coulibaly, Zana (2016) "Examining the Effect of Introducing a Link from Electrical Excitation to Calcium Dynamics in a Cardiomyocyte," *Spora: A Journal of Biomathematics*: Vol. 2: Iss. 1, .

DOI: <http://doi.org/10.30707/SPORA2.1Angeloff>

Available at: <https://ir.library.illinoisstate.edu/spora/vol2/iss1/6>

This Mathematics Research is brought to you for free and open access by ISU ReD: Research and eData. It has been accepted for inclusion in Spora: A Journal of Biomathematics by an authorized editor of ISU ReD: Research and eData. For more information, please contact [ISUReD@ilstu.edu](mailto:ISUReD@ilstu.edu).

---

# Examining the Effect of Introducing a Link from Electrical Excitation to Calcium Dynamics in a Cardiomyocyte

## Cover Page Footnote

These results were obtained as part of the REU Site: Interdisciplinary Program in High Performance Computing ([hpcreu.umbc.edu](http://hpcreu.umbc.edu)) in the Department of Mathematics and Statistics at the University of Maryland, Baltimore County (UMBC), in Summer 2016. This program is funded by the National Science Foundation (NSF), the National Security Agency (NSA), and the Department of Defense (DOD), with additional support from UMBC, the Department of Mathematics and Statistics, the Center for Interdisciplinary Research and Consulting (CIRC), and the UMBC High Performance Computing Facility (HPCF). HPCF is supported by the U.S. National Science Foundation through the MRI program (grant nos. CNS-0821258 and CNS-1228778) and the SCREMS program (grant no. DMS-0821311), with additional substantial support from UMBC. Co-author Uchenna Osia was supported in part by the UMBC National Security Agency (NSA) Scholars Program through a contract with the NSA. Graduate assistant Jonathan Graf was supported by UMBC.

## Authors

Kallista Angeloff, Carlos A. Barajas, Alexander Middleton, Uchenna Osia, Jonathan S. Graf, Matthias K. Gobbert, and Zana Coulibaly

# Examining the Effect of Introducing a Link from Electrical Excitation to Calcium Dynamics in a Cardiomyocyte

Kallista Angeloff<sup>1</sup>, Carlos Barajas<sup>2</sup>, Alexander Middleton<sup>3</sup>, Uchenna Osia<sup>4</sup>, Jonathan S. Graf<sup>5</sup>, Matthias K. Gobbert<sup>5,\*</sup>, Zana Coulibaly<sup>6</sup>

\*Correspondence:  
Prof. Matthias K. Gobbert,  
Dept. of Mathematics and  
Statistics, University of  
Maryland, Baltimore County,  
1000 Hilltop Circle,  
Baltimore, MD 21250, USA  
gobbert@umbc.edu

## Abstract

Calcium dysregulation is a significant cause of fatal cardiac arrhythmias, but it is an incompletely understood phenomenon and difficult to predict. Cardiac calcium levels can be modeled as a system of partial differential equations linking the electrical excitation, calcium signaling, and mechanical contraction dynamics of the heart. A complete calcium-induced calcium release model uses reaction-diffusion equations to fully link these three systems. Simulations examine the effect of introducing the link from calcium signaling to electrical excitation. In particular, we perform a parameter study on the strength of the feedback connection with both links between calcium signaling and electrical excitation enabled. Simulations indicate that the feedback and feedforward between electrical excitation and calcium signaling can influence the voltage in a physiologically realistic way.

**Keywords:** Calcium-induced calcium release, Cardiomyocytes, Contractile cardiac dynamics, Chemical cardiac dynamics, Electrical cardiac dynamics

## 1 Introduction

Heart disease is currently the leading cause of death in the United States, according to the Centers for Disease Control and Prevention [4]. Recent studies have shown that cardiac arrhythmias result from the disruption of the very tight coupling between the electrical, calcium, and mechanical properties of the heart [21]. The current treatment for cardiac arrhythmia, mild or otherwise, is surgical implantation of a pacemaker to artificially stimulate the electrical patterns which would be regulated by calcium levels in a healthy heart. To date, no medication has been developed that has proven to be effective in more than a handful of cases [18, 22].

Though devices like pacemakers have shown to help reduce the death rate due to arrhythmia, they do not prevent onset arrhythmia. A more in-depth understanding of the calcium dynamics may yield new methods in the realm of drug therapy. In order to better study the heart, we examine individual cells and three components associated with the dynamics: electrical excitation, calcium signaling, and mechanical contraction. These three systems are coupled together as seen in Figure 1.1 with

calcium signaling being the central dynamic component between the electrical excitation and mechanical contraction. It has been shown that the dysregulation of the interaction between these three systems is a precursor to cardiac arrhythmias [8, 17]. In particular, the disruption of the bi-directional coupling between calcium and electrical system can result in alternans (unwanted oscillation of the cell's calcium and electrical activity) [6, 21]. These alternans often precede an arrhythmia. Our goal is to obtain an insight into the delicate electro-chemical balance at the scale of a cardiomyocyte by expanding upon a model of calcium-induced calcium release to include the feedback-feedforward between the calcium and electrical systems.

The links shown in Figure 1.1 each represent a physiological component of the potential for *calcium-induced calcium release (CICR)* inside the cardiac cell. The solid line for link ① refers to a link from the electrical to the calcium system, whose behavior was the focus of the simulations in [1], while the dotted line for link ② is the link from the calcium to the electrical system, whose effect is the focus of the present simulations. The dashed lines labeled ③ and ④ are the links between the calcium and the mechanical system, whose model is introduced in this paper.

In normal conditions, the periodic nonarrhythmic contraction and relaxation of a cardiac myocyte is governed by periodic action potentials (cell's membrane depolar-

<sup>1</sup>Department of Atmospheric Sciences, University of Washington, <sup>2</sup>Department of Mathematics and Computer Science, Olivet College, <sup>3</sup>Department of Mathematics, Winthrop University, <sup>4</sup>Department of Computer Science and Electrical Engineering, UMBC, <sup>5</sup>Department of Mathematics and Statistics, UMBC, <sup>6</sup>Department of Pharmacology, University of California, Davis

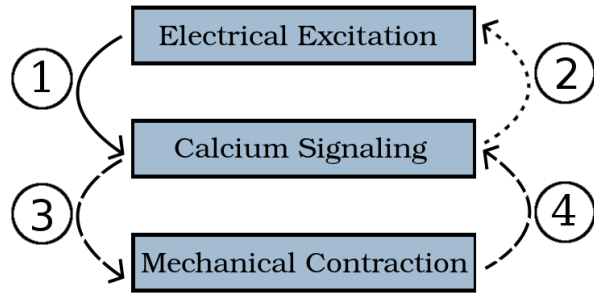


Figure 1.1: The calcium-mediated contractile rhythm of a given cardiomyocyte is a function of three coupled dynamics: electrical excitation, calcium signaling, and mechanical contraction. Their links are labeled ① to ④ for reference throughout the text.

ization and repolarization). In a regular functioning cardiac myocyte, the depolarization (increase in voltage) of the cell's membrane is due to an influx of sodium ions. The depolarization of the cell's membrane causes L-type calcium channels (LCC) to open thus causing an influx of calcium ions ( $\text{Ca}^{2+}$ ) into the cell. The influx of calcium ions inside the cell causes a localized increase in calcium concentration. Inside the heart cell, calcium ions are primarily stored in the sarcoplasmic reticulum (SR). The SR has calcium sensitive sites called calcium release units (CRUs) which, when the concentration of calcium is high enough, release calcium into the cytosol of the cell. The depolarization of the cell membrane also occurs when calcium ions are pumped out of the cell and sodium ions are pumped into the cell through the sodium calcium exchanger. While these system processes are interacting, calcium is also binding and unbinding to immobile contractile proteins inside of the cytosol. The contractile proteins are attached to muscular strands known as sarcomere and the cell expansion and contraction relates to the amount of calcium bound in this fashion. Repolarization of the membrane (decrease of the membrane voltage) occurs afterwards due to the activity of sodium/potassium pumps. The cell relaxation occurs when most of the calcium ions are pumped back into the SR through SR pumps. A closer analysis of these interactions is presented inside Section 2.

We represent the fully coupled electrical excitation, calcium signaling, and mechanical contraction components of the calcium and electrical dynamics by a system of eight time-dependent coupled partial differential equations (PDEs). The calcium signaling is described by five PDEs modeling concentrations of calcium ions and buffer species in the cytosol and SR. The electrical excitation, connected to the calcium system by links ① and ②, is represented by two PDEs: one representing voltage

and one representing the concentration of an additional electrolyte, potassium. The mechanical contraction, connected to the calcium system by links ③ and ④, is described by a final PDE representing the concentration of actively linked contractile proteins in the cytosol. A full description of the mathematical model is presented in Section 3.

We use numerical methods to perform simulations of this system of time-dependent, coupled, parabolic partial differential equations. The long time simulations required demand sophisticated numerical methods. We use a method of lines (MOL) approach and use the finite volume method (FVM) for the spatial discretization and the numerical differentiation formulas (NDFk) for time stepping. A memory efficient parallel implementation of this is done in C using MPI (Message Passing Interface, the most popular parallel communications library [16]) commands for parallel computing. A more detailed overview of the numerical methods be found in Section 4.

In Section 5, we present simulations of our model that examine back and forth interaction between the electrical excitation and calcium signaling systems. The simulations use as domain an elongated three-dimensional hexahedron that captures the key feature of a heart cell. Figure 1.2 shows the distances of the  $z$ -planes of CRUs being  $\Delta z_s$  apart, and the location of CRUs on each  $z$ -plane on a rectangular lattice with distances  $\Delta x_s$  and  $\Delta y_s$ . In Section 5.1, we show behavior with only the feedforward connection in which the electrical excitation impacts the calcium signaling, link ① in Figure 1.1. In Section 5.2 we analyze the impact of introducing the feedback connection enabling the calcium signaling to impact the electrical excitation in our model, that is, both link ① and link ② in Figure 1.1 are turned on. To do this, we modify the parameter that turns on and off the feedback connection,  $\omega$ , and study the influence of different strengths of this feedback. This study examines the impact of this change on concentration of calcium in both the cytosol and SR as well as the the average voltage in the cell. We also show figures with the open CRUs at various time values and figures with the concentration of calcium in the cytosol at various time values.

Finally, Section 6 summarizes this work and presents opportunities for future work. Simulations indicate that the feedback and feedforward between electrical excitation and calcium signaling can influence the voltage in a physiologically realistic way. That is, the simulated action potential is qualitatively similar to an experimental range and duration. The interplay between the strengths of the feedback and feedforward links of electrical excitation and calcium signaling and impact of the mechanical contraction components can now be studied.



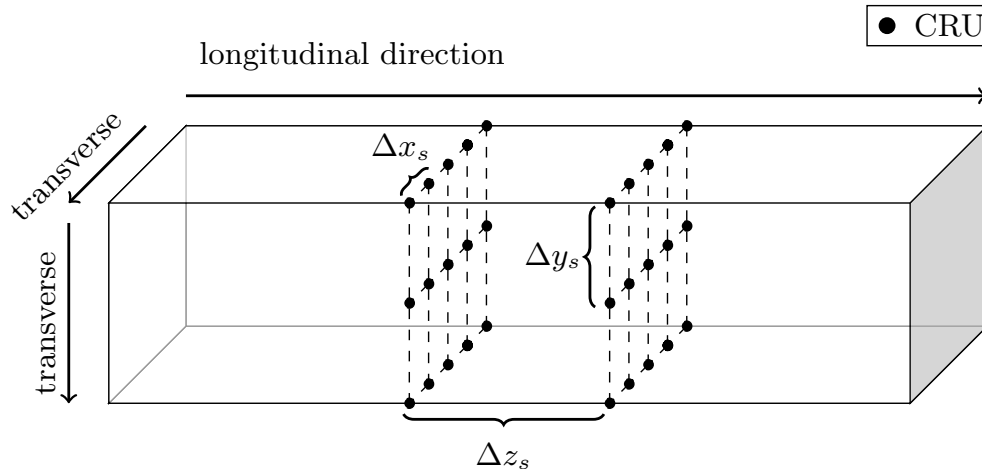


Figure 1.2: The CRU lattice with spacings  $\Delta x_s$ ,  $\Delta y_s$ , and  $\Delta z_s$  throughout the three-dimensional domain.

## 2 Background

The general structure of cardiomyocytes on the heart can be seen in Figure 2.1(a). The general shape of the cardiac cell is rectangular with several T-tubules along the side of the cell. The light pink areas of Figure 2.1(a) represent the cellular membrane of the cardiomyocyte. The muscle fibers run parallel to the contractile proteins of the cardiac cell. The dark splotches are the cell nuclei associated with their respective cell. Inside the cardiomyocyte is the sarcoplasmic reticulum (SR), a type of container that contains both calcium ions and calsequestrin (CSQ). The release of calcium from the SR into the cytosol occurs via calcium release units (CRUs) on the SR. Once the concentration is high enough, the CRUs will begin to open; this process is called *sparking*. Sparking is the scattered, local simultaneous opening of a small number of CRUs [5]. The fluorescent dye is mixed in the cytosol and used to make the calcium more visible during lab experiments; the dye diffuses through the cytosol interacting with and binding to calcium in the cytosol.

How these components combine to affect small strands of muscle fiber and cause cell pulsation is shown in Figure 2.2(a). The sodium-calcium electrical exchanger, labeled as NCX near the top of Figure 2.2(a), pushes a calcium ion out of the cell while bringing three sodium ions into cell. Calcium leaving the cell is part of a feedback mechanism, designated as link ② in Figure 1.1, by which the electrical properties of the heart are influenced by calcium concentration in the cytosol. When the concentration begins to change, it leads to a phenomenon in which regular depolarizations of the cell plasma membrane happen; the depolarization induces spontaneous action potential, causing the L-type Calcium Channels (LCC) to open. This feedforward mechanism, represented by link

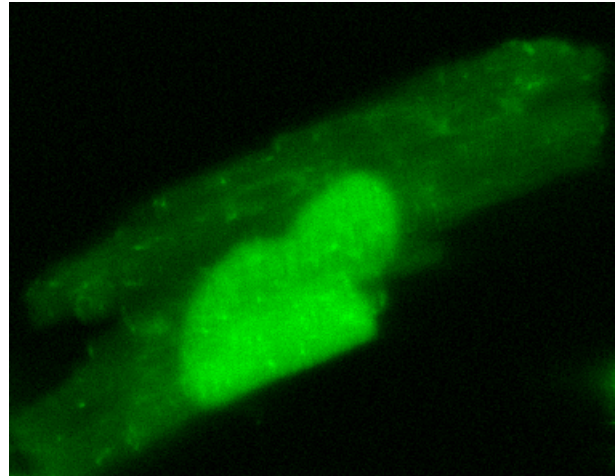
① in Figure 1.1, is another one-way coupling which allows for the electrical aspect of the cardiac cell to have an influence on the calcium concentration of the cytosol. These two methods result in a two-way coupling between the electrical excitation system and calcium signaling in the cell.

As the CRUs release more calcium into the cytosol, the spike in concentration can trigger neighboring CRUs to open as well possibly leading to the cascading effect depicted in Figure 2.2(b). This wave can propagate until the SR stores are depleted of calcium, which are then replenished via an intracellular pump on the SR. When calcium begins to pour into the cytosol, the concentration begins to rise, triggering another wave event within the cell: calcium release [7]. This behavior is known as *calcium-induced calcium release (CICR)*. As calcium diffuses through the cytosol, it reacts with other chemical species; among them, in this model, are the fluorescent dye fluoro-4 and tropomyosin contractile proteins.

The contraction and expansion of the cell's shape is a result of the contractile proteins; the contractile proteins, called *tropomyosin*, located in the bottom right-hand corner of Figure 2.2(a), are comprised of troponin, actin, myosin heads, and attached to a sacromere. When calcium binds to the troponin complex, the myosin heads are free to converge to the actin bridge; when the myosin heads come in contact with the bridge the striated muscle, the sacromere, which is parallel to the tropomyosin, contracts. This myosin contraction is the physical process through which the cell expands and contracts; when these contractions are performed in unison with other cardiac cells, that section of the heart pulses. This process of calcium causing heart contractions presents the first coupling between the calcium and the contractile nature of a heart cell; these chemical interactions are a feedforward

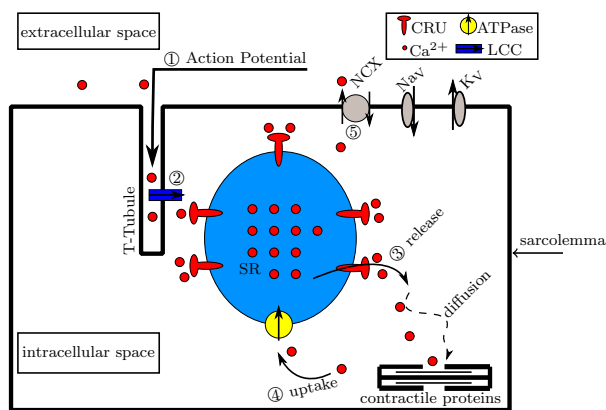


(a) Cardiac cell structure

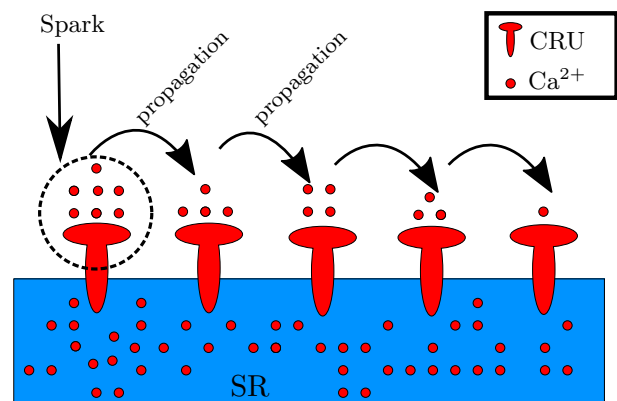


(b) Calcium filled cardiomyocyte

Figure 2.1: (a) A conglomerate of cardiac cells. The muscle fibers of each heart cell contract in response to the change in shape of contractile proteins, in turn mediated by calcium levels in the cytosol. These muscle fibers can be seen as darker striations throughout the cell. (b) An individual rabbit cardiomyocyte illuminated by a fluorescent dye. Experiment conducted by Dr. Kenneth Spitzer (University of Utah, personal communication, June 2010).



(a) Cellular space



(b) Calcium wave triggering

Figure 2.2: (a) The T-tubules enfolds the L-type calcium channels (LCC) in the cell's plasma membrane. Periodic membrane depolarizations allow calcium to pass into the cytosol. (b) Calcium is released from the calcium release units (CRUs) on the SR and begin the cascading calcium release that starts calcium wave propagation.

process and represented by link ③ in Figure 1.1. Once calcium is bound to the complex, the bridge-like structure deforms, causing the rate at which calcium unbinds to decrease. Conceptually the change in the troponin complex causes the bridge to hang onto the calcium for longer. When the calcium is relinquished from the bridge, this increases the concentration of calcium in the cytosol as a feedback process, which is represented by link ④ in Figure 1.1.

### 3 Model

In this section, we present the equations of the complete model along with parameter tables and descriptions of how the equations represent the physiological components. The PDEs of the model are (3.1), (3.2) with  $n_{sc} = 3$ , (3.3), (3.4) with  $n_{ss} = 1$ , (3.12), and (3.13) yielding a total number of  $n_s = 4 + n_{sc} + n_{ss} = 8$  PDEs. The eight species of the model are: calcium in the cytosol  $c(\mathbf{x}, t)$ , a florescent dye  $b_1^{(c)}(\mathbf{x}, t)$ , a contractile protein (troponin)  $b_2^{(c)}(\mathbf{x}, t)$ , a contractile force  $b_3^{(c)}(\mathbf{x}, t)$ , calcium in the SR  $s(\mathbf{x}, t)$ , calsequestrin in the SR  $b_1^{(s)}(\mathbf{x}, t)$ , voltage  $V(\mathbf{x}, t)$ , and potassium  $n(\mathbf{x}, t)$ . Section 3.1 describes the calcium signaling portion of the model without the presence of electrical excitation or mechanical contraction that was originally introduced in [12, 14], extended in [13], and its numerics discussed with  $n_{sc} = 2$  in [9, 10, 19, 20]. Section 3.2 introduces the electrical excitation that is connected to the calcium signaling in both the feedforward and feedback directions represented by link ① and link ② in Figure 1.1. Link ① from electrical system to the calcium dynamics was first established in [1]. Finally, Section 3.3 completes the fully linked model with the addition of the mechanical contraction component that is also connected to the calcium signaling in both the feedback and feedforward directions represented by links ③ and ④ in Figure 1.1. The effects of cell contraction are implemented via a pseudo-mechanical model, as in [3], which describes force in terms of the proportion of actively connected contractile proteins.

#### 3.1 Calcium signaling

We start with a system of reaction diffusion PDEs

$$\begin{aligned} \frac{\partial c}{\partial t} = & \nabla \cdot (D_c \nabla c) + \sum_{i=1}^{n_{sc}} R_i^{(c)} \\ & + (J_{CRU} + J_{leak} - J_{pump}) \\ & + \kappa J_{LCC} + J_{mleak} - J_{mpump}, \end{aligned} \quad (3.1)$$

$$\frac{\partial b_i^{(c)}}{\partial t} = \nabla \cdot (D_{b_i^{(c)}} \nabla b_i^{(c)}) + R_i^{(c)} \quad (3.2)$$

for  $i = 1, \dots, n_{sc}$ ,

$$\begin{aligned} \frac{\partial s}{\partial t} = & \nabla \cdot (D_s \nabla s) + \sum_{j=1}^{n_{ss}} R_j^{(s)} \\ & - \gamma(J_{CRU} + J_{leak} - J_{pump}), \end{aligned} \quad (3.3)$$

$$\frac{\partial b_j^{(s)}}{\partial t} = \nabla \cdot (D_{b_j^{(s)}} \nabla b_j^{(s)}) + R_j^{(s)} \quad (3.4)$$

for  $j = 1, \dots, n_{ss}$ , where  $c(\mathbf{x}, t)$  and  $s(\mathbf{x}, t)$  represent the concentrations of calcium in the cytosol and SR, respectively.  $b_i^{(c)}(\mathbf{x}, t)$  and  $b_j^{(s)}(\mathbf{x}, t)$  represent the concentration of each buffer species in the cytosol SR, respectively. Table 3.1 collects the variables with their units as well as the values of parameters in the PDEs of the calcium system.  $D_c, D_s, D_{b_i^{(c)}},$  and  $D_{b_j^{(s)}}$  are diffusion matrices for  $\text{Ca}^{2+}$  in the cytosol,  $\text{Ca}^{2+}$  in the SR, and each buffer species in the cytosol and SR, respectively. While each buffer species programmatically possesses a diffusion matrix (following the template of (3.2) and (3.4)), not all species are mobile; hence the diffusion matrices for some species are zero matrices in Table 3.1.

The reaction terms  $R_i^{(c)}$  and  $R_j^{(s)}$  describe the reactions between calcium and the buffer species. They are the connections between (3.1) and (3.2), and between (3.3) and (3.4). More precisely,

$$R_i^{(c)} = -k_{b_i^{(c)}}^+ c b_i^{(c)} + k_{b_i^{(c)}}^- (b_{i,total}^{(c)} - b_i^{(c)}), \quad (3.5)$$

for  $i = 1, \dots, n_{sc}$ , model the reactions between cytosolic  $\text{Ca}^{2+}$  and each cytosolic buffer species, and

$$R_j^{(s)} = -k_{b_j^{(s)}}^+ s b_j^{(s)} + k_{b_j^{(s)}}^- (b_{j,total}^{(s)} - b_j^{(s)}), \quad (3.6)$$

for  $j = 1, \dots, n_{ss}$ , model the reactions between SR  $\text{Ca}^{2+}$  and each SR buffer species. The amounts of “free” calcium ions,  $c(\mathbf{x}, t)$  and  $s(\mathbf{x}, t)$  in (3.1) and (3.3), respectively, and of “free” buffer species in (3.2) and (3.4), respectively, are determined by these reactions: whatever has not been bound by a reaction is the concentration remaining. In the cytosol, two buffer species are considered: a fluorescent dye,  $b_1^{(c)}(\mathbf{x}, t)$ , and a contractile protein troponin,  $b_2^{(c)}(\mathbf{x}, t)$ . We will revisit the subject of troponin in our extension of this model to include the pseudo-mechanical dynamics of the cell. In the SR, a single buffer species is considered: calsequestrin,  $b_1^{(s)}(\mathbf{x}, t)$ , a calcium-binding protein which helps maintain the SR calcium reserves at a much higher concentration than the cytosol (i.e., prevents too great a loss through diffusion).

The flux terms  $J_{CRU}, J_{leak},$  and  $J_{pump}$  in (3.1) describe the calcium-induced release of  $\text{Ca}^{2+}$  into the cytosol from the SR, the continuous leak of  $\text{Ca}^{2+}$  into the cytosol from the SR, and the pumping of  $\text{Ca}^{2+}$  back into the SR from

Table 3.1: Variables and parameters for calcium signaling: PDEs.

Variable	Definition	Values/Units
$\mathbf{x}$	spatial position variable $(x, y, z)$	$\mu\text{m}$
$t$	time variable	seconds
$c(\mathbf{x}, t)$	cytosol calcium concentration	$\mu\text{M}$
$s(\mathbf{x}, t)$	SR calcium concentration	$\mu\text{M}$
$n_{sc}$	number of cytosol $\text{Ca}^{2+}$ buffer species	2
$n_{ss}$	number of SR $\text{Ca}^{2+}$ buffer species	1
$b_1^{(c)}_{total}$	total amount of $b_1^{(c)}(\mathbf{x}, t)$ , dye, in cytosol	50 $\mu\text{M}$
$b_2^{(c)}_{total}$	total amount of $b_2^{(c)}(\mathbf{x}, t)$ , troponin, in cytosol	123 $\mu\text{M}$
$b_1^{(s)}_{total}$	total amount of $b_1^{(s)}(\mathbf{x}, t)$ , calsequestrin, in SR	6000 $\mu\text{M}$
$D_c$	cytosolic calcium diffusion coefficient matrix	diag(0.15, 0.15, 0.3)
$D_s$	SR calcium diffusion coefficient matrix	diag(0.78, 0.78, 0.78) $\mu\text{m}^2/\text{ms}$
$D_{b_1^{(c)}}$	cytosol buffer diffusion coefficient matrix ( $i = 1$ , dye)	diag(0.01, 0.01, 0.02) $\mu\text{m}^2/\text{ms}$
$D_{b_2^{(c)}}$	cytosol buffer diffusion coefficient matrix ( $i = 2$ , troponin)	diag(0.00, 0.00, 0.00) $\mu\text{m}^2/\text{ms}$
$D_{b_1^{(s)}}$	SR buffer diffusion coefficient matrix ( $i = 1$ , calsequestrin)	diag(0.00, 0.00, 0.00) $\mu\text{m}^2/\text{ms}$
$R_i^{(c)}, R_j^{(s)}$	reactions of cytosol, SR $\text{Ca}^{2+}$ with buffers	$\mu\text{M}/\text{ms}$
$k_{b_1^{(c)}}^+$	forward reaction coefficient for $b_1^{(c)}$ , dye	$80 \times 10^{-3} \mu\text{M}/\text{ms}$
$k_{b_2^{(c)}}^+$	forward reaction coefficient for $b_2^{(c)}$ , troponin	$100 \times 10^{-3} \mu\text{M}/\text{ms}$
$k_{b_1^{(s)}}^+$	forward reaction coefficient for $b_1^{(s)}$ , calsequestrin	$39 \times 10^{-3} \mu\text{M}/\text{ms}$
$k_{b_1^{(c)}}^-$	reverse reaction coefficient for $b_1^{(c)}$ , dye	$90 \times 10^{-3} \text{ms}^{-1}$
$k_{b_2^{(c)}}^-$	reverse reaction coefficient for $b_2^{(c)}$ , troponin	$100 \times 10^{-3} \text{ms}^{-1}$
$k_{b_1^{(s)}}^-$	reverse reaction coefficient for $b_1^{(s)}$ , calsequestrin	$78 \text{ms}^{-1}$
$\gamma$	ratio of volume of cytosol to SR	14
$c_0$	basal cytosol calcium concentration	0.1 $\mu\text{M}$
$J_{pump}$	calcium transfer from cytosol to SR	$\mu\text{M}/\text{ms}$
$J_{leak}$	calcium leak from SR	$\mu\text{M}/\text{ms}$
$V_{pump}$	maximum pump rate	2 to 6 $\mu\text{M}/\text{ms}$
$K_{pump}$	pump sensitivity to $\text{Ca}^{2+}$	0.184 $\mu\text{M}$
$n_{pump}$	Hill coefficient for pump function	4.0
$s_0$	initial SR calcium concentration	1,000 to 10,000 $\mu\text{M}$
$J_{CRU}$	calcium flux from SR to cytosol via CRUs	$\mu\text{M}/\text{ms}$
$\mathcal{O}$	gating function for $J_{CRU}$	1
$J_{prob}$	probability of CRU opening	0 to 1
$\mathbf{x}$	three-dimensional vector for CRU location	$\mu\text{m}$
$\hat{\sigma}$	maximum rate of release	100 to 200 $\mu\text{M} \mu\text{m}^3/\text{ms}$
$u_{rand}$	uniformly distributed random variable	0 to 1
$n_{prob}$	Hill coefficient for probability function	1.6
$P_{max}$	maximum probability for release	0.3
$K_{prob_c}$	sensitivity of CRU to cytosol calcium	5 to 15 $\mu\text{M}$
$K_{prob_s}$	sensitivity of CRU to SR calcium	200 to 550 $\mu\text{M}$

the cytosol. The terms  $J_{LCC}$ ,  $J_{leak}$ , and  $J_{mpump}$  describe the fluxes of calcium into and out of the cell via the plasma membrane. The coupling between (3.1) and (3.3) is achieved by the three flux terms shared by both.

More precisely,  $J_{LCC}$ ,  $J_{leak}$ , and  $J_{mpump}$  in (3.1) describe the fluxes of calcium into and out of the cell via the plasma membrane.  $J_{pump}$  replenishes the calcium stores in the SR; it increases SR calcium concentration by decreasing cytosol calcium concentration.  $J_{leak}$  is a continuous leakage of those SR calcium stores into the cytosol; it increases cytosol concentration by decreasing SR calcium concentration. The pump term

$$J_{pump}(c) = V_{pump} \left( \frac{c^{n_{pump}}}{K_{pump}^{n_{pump}} + c^{n_{pump}}} \right) \quad (3.7)$$

is thus a function of cytosol calcium  $c(\mathbf{x}, t)$ . The leak term  $J_{leak}$  is a constant defined by

$$J_{leak} = J_{pump}(c_0), \quad (3.8)$$

which balances  $J_{pump}(c)$  at basal level  $c_0 = 0.1 \mu\text{M}$  of cytosol calcium. The pump term  $J_{pump}$ , a function of cytosolic calcium  $c(\mathbf{x}, t)$ , consists of the maximum pump velocity  $V_{pump}$  multiplied against the relationship between  $c(\mathbf{x}, t)$  and the pump sensitivity  $K_{pump}$ ; the exponent  $n_{pump}$  refers to the Hill coefficient (quantifying the degree of cooperative binding) for the pump function. This has the practical effect of multiplying the maximum possible pump velocity against a number between 0 and 1, exclusive.  $J_{leak}$ , which continuously leaks calcium into the cytosol from the SR, is simply  $J_{pump}$  evaluated at the basal cytosolic calcium concentration  $c_0 = 0.1 \mu\text{M}$ . As noted,  $J_{pump}$  balances  $J_{leak}$  in the absence of sparking. It can also balance  $J_{CRU}$  under conditions of active calcium release.

The term  $J_{CRU}$  in (3.1) is the  $\text{Ca}^{2+}$  flux into the cytosol from the SR via each individual point source at which a CRU has been assigned. The effect of all CRUs is modeled as a superposition such that

$$J_{CRU}(c, s, \mathbf{x}, t) = \sum_{\hat{\mathbf{x}} \in \Omega_s} \hat{\sigma} \frac{s-c}{s_0-c_0} \mathcal{O}(c, s) \delta(\mathbf{x} - \hat{\mathbf{x}}) \quad (3.9)$$

with

$$\mathcal{O}(c, s) = \begin{cases} 1 & \text{if } u_{rand} \leq J_{prob}, \\ 0 & \text{if } u_{rand} > J_{prob}, \end{cases} \quad (3.10)$$

where

$$J_{prob}(c, s) = P_{max} \left( \frac{c^{n_{prob}}}{K_{prob_c}^{n_{prob}} + c^{n_{prob}}} \right) \left( \frac{s^{n_{prob}}}{K_{prob_s}^{n_{prob}} + s^{n_{prob}}} \right). \quad (3.11)$$

Here, the effect of each CRU is modeled as a product of three terms:

- (i) Similarly to how in  $J_{pump}$  the maximum pump rate is scaled against the concentration of available cytosol calcium, the maximum rate of  $\text{Ca}^{2+}$  release  $\hat{\sigma}$  is scaled here against the ratios of calcium concentrations in the cytosol and in the SR.
- (ii) Following the same pattern a maximum value multiplied against some scaling proportion between 0 and 1 the gating function  $\mathcal{O}$  has the practical effect of “budgeting” the calcium SR stores such that when the stores are low, the given CRU becomes much less likely to open; each CRU is assigned a uniformly distributed random value, which is compared to the single value returned by the CRU opening probability  $J_{prob}$  to determine whether or not the given CRU will open.
- (iii) The Dirac delta distribution  $\delta(\mathbf{x} - \hat{\mathbf{x}})$  models each CRU as a point source for calcium release.

### 3.2 Electrical excitation

The membrane potential of the cell depends on both the cytosol calcium ion concentration and also on the cytosol potassium ion ( $\text{K}^+$ ) concentration [3, 15]. While a complete description of the relationship between electrolytes and membrane potential is beyond the scope of this paper, note the  $\omega$  term, an addition of our model which introduces a dependency on  $c$  to complete the coupling between the electrical and chemical systems. Table 3.2 collects the variables and parameters for electrical excitation.

The  $\text{Ca}^{2+}$  conductance is much faster than the  $\text{K}^+$  conductance, so the calcium conductance can be approximated as  $m_\infty$  or instantaneously steady-state at all times; the potassium conductance requires a separate description in (3.13)

$$\begin{aligned} \frac{\partial V}{\partial t} = \tau \frac{1}{C} & \left( I_{app} - g_L(V - V_L) \right. \\ & - g_{Ca} m_\infty(V) (V - V_{Ca}) \\ & \left. - g_K n(V - V_K) + \omega (J_{mpump} - J_{leak}) \right), \end{aligned} \quad (3.12)$$

$$\frac{\partial n}{\partial t} = \tau \lambda_n(V) [n_\infty(V) - n]. \quad (3.13)$$

The connection between (3.1) and (3.12), link ① in Figure 1.1, the link from the electrical system to the calcium system, comes through  $J_{LCC}$ , the only calcium flux term to involve voltage. Note the parameter  $\kappa$ , which is an external scaling factor for  $J_{LCC}$  rather than an intrinsic physiological component; if the value of  $\kappa$  is set to 0, the connection, link ① in Figure 1.1, is effectively switched off and the calcium dynamics are then modeled as though voltage were not involved

$$J_{LCC} = \frac{S g_{Ca} m_\infty(V - V_{Ca})}{2F}. \quad (3.14)$$

The surface area,  $S$ , of the cell is included in light of the fact that  $J_{LCC}$  describes the influx of calcium through L-type calcium channels (LCCs), which are present in the enclosing plasma membrane of the cell: the surface area of the cell is the surface area of the membrane.

We model the effect of cytosol calcium concentration on voltage by treating the calcium efflux term ( $J_{m_{pump}} - J_{m_{leak}}$ ) as equivalent to the sodium-calcium exchanger current: we are thus able to describe the current generated by the sodium-calcium exchange as a function of simple calcium loss.

The individual components of the calcium efflux term are near-duplicates in form of the earlier  $J_{pump}$  and  $J_{leak}$  functions in (3.7) and (3.8), respectively. As  $J_{pump}$  described the removal of calcium from the cytosol and its transfer into SR stores,

$$J_{m_{pump}}(c) = V_{m_{pump}} \left( \frac{c^{m_{n_{pump}}}}{K_{m_{pump}}^{m_{n_{pump}}} + c^{m_{n_{pump}}}} \right) \quad (3.15)$$

describes the removal of calcium from the cytosol and its transfer to outside the cell across the membrane. The leak term  $J_{leak}$  described a gradual leak of calcium into the cytosol from the SR, while  $J_{CRU}$  described an abrupt, high-concentration (high relative to the leak) release of calcium into the cytosol from the SR. Similarly,

$$J_{m_{leak}} = J_{m_{pump}}(c_0) \quad (3.16)$$

describes a gradual leak of calcium into the cytosol from outside the cell via the plasma membrane, while  $J_{LCC}$  describes a sudden spike of calcium release into the cytosol via the LCCs.

At this juncture, we extend the model to connect the chemical system to the electrical system, link ② in Figure 1.1, via the inclusion of the current generated by calcium leaving the cell via  $J_{m_{pump}}$  and  $J_{m_{leak}}$ , which directly affects the voltage. We collect and incorporate these as a single term, the calcium efflux ( $J_{m_{pump}} - J_{m_{leak}}$ ), and introduce  $\omega$  as a parameter for feedback strength in link ② in Figure 1.1, which is a scaling factor with the same essential function as  $\kappa$  in link ① in Figure 1.1 from (3.1): if it is set to 0, the only terms of (3.12) which depend on the cytosolic calcium concentration drop out, and the connection from calcium signaling to electrical excitation is severed.

### 3.3 Pseudo-mechanical contraction

We complete the proposed links of the model, ③ and ④ in Figure 1.1, by introducing feedback and feedforward terms for the contractile dynamics. We describe this as “pseudo-mechanical” because the domain itself is unchanged; in our model, the physical dimensions of the cell and the locations of the CRUs do not alter. We instead

model the contraction via the proportion of contractile proteins which have bound to calcium and changed shape as a result, which generates the force required for cell contraction. Table 3.3 collects the variables and parameters for pseudo-mechanical contraction.

The contractile proteins in question, though considered as a single species, are the combination of actin and myosin when linked via cross-bridges. This linkage is made possible by  $\text{Ca}^{2+}$  binding to troponin, the cytosol buffer species  $b_2^{(c)}(\mathbf{x}, t)$ : it is this binding that allows the actin-myosin cross-bridges to form. We therefore introduce a new cytosol species,  $b_3^{(c)}(\mathbf{x}, t)$ , to describe these actin-myosin cross-bridges, and construct a third cytosol reaction term:

$$R_{b_3}^{(c)} = -k_{b_3}^+ \left( \frac{b_{2,total}^{(c)} - b_2^{(c)}}{b_{2,total}^{(c)}} \right)^2 b_3^{(c)} + k_{b_3}^- (b_{3,total}^{(c)} - b_3^{(c)}). \quad (3.17)$$

Notice that this is not the same as the generic pattern for buffer species reaction terms from the initial model. There is no immediately clear dependence on cytosolic calcium  $c(\mathbf{x}, t)$ . However, while  $c(\mathbf{x}, t)$  is not explicitly included, it is present in the proportion involving troponin,  $b_3^{(c)}(\mathbf{x}, t)$ , which itself depends explicitly on cytosol calcium levels;  $R_{b_3}^{(c)}$ , like the other two reaction equations, does in fact depend on cytosol calcium concentration.

We modify the reaction equation for troponin as well. When troponin binds to  $\text{Ca}^{2+}$ , the protein as a whole, as noted, changes shape: not only does this allow actin-myosin cross-bridges to form, but it also traps the calcium in its connection to the troponin so that the disassociation rate decreases dramatically. To account for this, we add a shortening factor  $\varepsilon$  to describe how the separation of troponin and calcium has been physically, not chemically, impaired. Note, again, that  $R_{b_2}^{(c)}$  remains a function of cytosol calcium concentration  $c(\mathbf{x}, t)$ :

$$R_{b_2}^{(c)} = -k_{b_2}^+ c b_2^{(c)} + k_{b_2}^- \left( b_{2,total}^{(c)} - b_2^{(c)} \right) \frac{1}{\varepsilon} \quad (3.18)$$

with

$$\varepsilon = \exp \left( F_{max} k_s \left( \frac{b_{3,total}^{(c)} - b_3^{(c)} - [XB]_0}{b_{3,total}^{(c)} - [XB]_0} \right) \right). \quad (3.19)$$

This shortening factor  $\varepsilon$  links ③ and ④ in Figure 1.1. It refers back to the concentration of  $b_3^{(c)}(\mathbf{x}, t)$ , the actin-myosin cross-bridges, and to the force that their linkage generates. It is scaled by the maximum possible contractile force  $F_{max}$ , the actin stiffness  $k_s$ , and the proportion of active to inactive actin-myosin cross-bridges. Like  $\omega$  and  $\kappa$ ,  $\varepsilon$  is our point of control over the linkage between

Table 3.2: Variables and parameters for electrical excitation: gating functions and membrane potential.

Variable	Definition	Values/Units
$V(\mathbf{x}, t)$	membrane potential (voltage)	mV
$\tau$	scaling factor to fit action potential duration	$0.1 \mu\text{M} \mu\text{m}^3/\text{ms}$
$V_L$	equilibrium potential for leak conductance	-50 mV
$V_{Ca}$	equilibrium potential for $\text{Ca}^{2+}$ conductance	100 mV
$V_K$	equilibrium potential for $\text{K}^+$ conductance	-70 mV
$C$	membrane capacitance	$20 \mu\text{F}/\text{cm}^2$
$I_{app}$	applied current	$10 \mu\text{A}/\text{cm}^2$
$g_L$	maximum/instantaneous conductance for leak	$2 \text{ mmho}/\text{cm}^2$
$g_{Ca}$	max./instantaneous conductance for $\text{Ca}^{2+}$	$4 \text{ mmho}/\text{cm}^2$
$g_K$	max./instantaneous conductance for $\text{K}^+$	$8 \text{ mmho}/\text{cm}^2$
$m_\infty$	fraction of open calcium channels at steady state	0 to 1
$n(\mathbf{x}, t)$	fraction of open potassium channels	0 to 1
$n_\infty$	fraction of open potassium channels at steady state	1
$\lambda_n(V)$	rate constant for opening of $\text{K}^+$ channels	$\text{s}^{-1}$
$J_{LCC}$	influx of calcium into cell via L-type calcium channels	$\mu\text{M}/\text{ms}$
$S$	surface area of the cell	$3604.48 \mu\text{m}$
$F$	Faraday constant	$95484.56 \text{ C}/\text{mol}$
$\kappa$	scaling factor of $J_{LCC}$	0.01
$\omega$	feedback strength (scaling factor) for $\text{Ca}^{2+}$ efflux	$\mu\text{A ms}/\mu\text{M cm}^2$
$J_{m_{pump}}$	pump of calcium out from cell via L-type calcium channels	$\mu\text{M}/\text{ms}$
$J_{m_{leak}}$	leak of calcium out from cell via L-type calcium channels	$\mu\text{M}/\text{ms}$
$V_{m_{pump}}$	maximum pump rate	$1 \mu\text{M}/\text{ms}$
$m_{n_{pump}}$	membrane pump Hill coefficient	2
$K_{m_{pump}}$	membrane pump sensitivity	0.18

Table 3.3: Variables and parameters for mechanical contraction: new cytosol species reactions.

Variable	Definition	Values/Units
$b_3^{(c)}(\mathbf{x}, t)$	inactive actin-myosin cross-bridges [X]	$\mu\text{M}$
$[XB]$	active (linked) actin-myosin cross-bridges	$\mu\text{M}$
$[XB]_0$	initial concentration of active cross-bridges	$\mu\text{M}$
$k_{b_3^{(c)}}^+$	forward reaction coefficient for $b_3^{(c)}(\mathbf{x}, t)$ , actin-myosin cross-bridges	$0.04 \text{ ms}^{-1}$
$k_{b_3^{(c)}}^-$	reverse reaction coefficient for $b_3^{(c)}(\mathbf{x}, t)$ , actin-myosin cross-bridges	$0.01 \text{ ms}^{-1}$
$\varepsilon$	shortening factor	0 to 1
$k_s$	stiffness of actin filament	$0.025 \text{ N}/\text{m}$
$F_{max}$	maximum force generated by actin-myosin crossbridges	$120 \mu\text{N}$



systems: if the exponent is 0, the overall value simply turns to 1, and  $R_{b_2}^{(c)}$  reverts to its earlier form (3.5).

The addition of these two reaction terms connects the three components of our model. The calcium signaling is linked to the pseudo-mechanical contraction through the cross-bridge term, and the pseudo-mechanical contraction is in turn connected to the calcium signaling through the inclusion of the cytosol calcium concentration in the modified reaction equation for troponin. Thus all links ①, ②, ③, and ④ in Figure 1.1 are established, and thus the three systems of the model are fully linked.

## 4 Numerical Method

In order to do calculations for the CICR model, we need to solve a system of time-dependent parabolic partial differential equations (PDEs). These PDEs are coupled by several non-linear reaction and source terms. For the simulations in Section 5, we need six species, thus we have  $n_s = 6$  coupled PDEs. The domain in our model is a hexahedron with isotropic CRU distribution as seen in Figure 1.2. Taking a method of lines (MOL) approach to spatially discretize this model, we use the finite volume method (FVM) as the spatial discretization, with  $N = (N_x + 1)(N_y + 1)(N_z + 1)$  control volumes. Applying this to the case of the  $n_s$  PDEs results in a large system of ordinary differential equations (ODEs). A MOL discretization of a diffusion-reaction equations with second-order spatial derivatives results in a stiff ODE system. The time step size restrictions, due to the CFL condition, are considered too severe to allow for explicit time-stepping methods. This necessitates the use of a sophisticated ODE solver such as the family of numerical differentiation formulas (NDF $k$ ). Our stiff ODEs, which needs to use an implicit ODE method, require the solution of a non-linear system. We use Newton's Method as non-linear solver, and at each Newton step we use BiCGSTAB as the linear solver. Complete details of the numerical method can be found in [11, 19].

The implementation of this model is done in C using MPI to parallelize computations. Parallelization is accomplished through block-distribution all large arrays to all MPI processes. MPI commands such as `MPI_Isend` and `MPI_Irecv`, which are non-blocking point-to-point communication commands, send messages between neighboring processes. The collective command `MPI_Allreduce` is used for the computation of scalar products and norms.

The spatial discretization of the application problem using the total number of species,  $n_s = 6$ , and the finite volume method with  $N$  control volumes results in a system of non-linear ordinary differential equations (ODEs) with  $n_{eq} = n_s N$  degrees of freedom (DOF). Table 4.1

shows the number of degrees of freedom for different mesh sizes for this problem. Simulation times depend heavily on the number of time steps taken. For each of the mesh sizes, the total number of time steps is listed. Note that the number of time steps increases for finer meshes, but the increase is not as large at the increase in DOF. We are using a matrix-free method that minimizes memory usage by not storing any system matrix; the code with the NDF $k$  method of orders  $1 \leq k \leq 5$  requires then, including all auxiliary method vectors, the storage of only 17 arrays of significant size  $n_{eq}$ . Table 4.1 also shows predicted memory usage for the 6 species simulation on each mesh as well as observed total memory used. The predicted memory is a realistic underestimate of the total memory observation.

## 5 Results

In this work, we focus on the electrical excitation and calcium signaling link impacts. Simulations necessary for this rely on six species: calcium in the cytosol  $c(\mathbf{x}, t)$ , a fluorescent dye  $b_1^{(c)}(\mathbf{x}, t)$ , a contractile protein (troponin)  $b_2^{(c)}(\mathbf{x}, t)$ , calcium in the SR  $s(\mathbf{x}, t)$ , voltage  $V(\mathbf{x}, t)$ , and potassium  $n(\mathbf{x}, t)$ . Thus, the  $n_s = 6$  PDEs of the model are (3.1), (3.2) with  $n_{sc} = 2$ , (3.3), (3.12), and (3.13) as described in Section 3. We consider for this the domain  $\Omega = (-6.4, 6.4) \times (-6.4, 6.4) \times (-32.0, 32.0)$  in Figure 1.2 that captures the key feature of the elongated shape of a heart cell. With the physiological constants  $\Delta x_s = 0.8$ ,  $\Delta y_s = 0.8$ , and  $\Delta z_s = 2.0$  for the CRU spacings, we have therefore a CRU lattice of  $15 \times 15 \times 31 = 6,975$  CRUs throughout the interior of the cell.

When examining the calcium behavior in the cytosol this model has demonstrated three main behaviors: sparking, wave, and blowup. Sparking is the behavior in which only small, localized release of calcium occur. That is, there is no propagation or build up of calcium in the cell, only sparks. When waves of calcium move through the cell, propagated by the calcium-induced calcium release, the behavior is classified as wave. So called blowup occurs when the cell becomes flooded with calcium and maintained that high concentration of calcium until the final time.

Studies in [1] established which of the calcium behaviors result under different parameter sets in relation to electrical excitation. We start by selecting a set of parameters that resulted in each of the three primary behaviors, Table 5.1. Recall here that  $\kappa$  in (3.1) turns on the link ① in Figure 1.1 from the electrical excitation to the calcium signaling system.

To visualize the solutions, we present five different types of plots: CRU plots, isosurface plots, line scans, voltage plots and SR plots. Each of these plots displays

Table 4.1: Sizing study with  $n_s = 6$  species using double precision arithmetic, listing the mesh resolution  $N_x \times N_y \times N_z$ , the number of control volumes  $N = (N_x + 1)(N_y + 1)(N_z + 1)$ , the number of degrees of freedom (DOF)  $n_{eq} = n_s N$ , the number of time steps taken by the ODE solver, and the predicted and observed memory usage in GB for a one-process run.

Resolution	$N$	DOF $n_{eq}$	number of time steps	memory usage (GB)	
				predicted	observed
$16 \times 16 \times 64$	18,785	112,710	32,047	0.01	0.25
$32 \times 32 \times 128$	140,481	842,886	43,473	0.11	0.64
$64 \times 64 \times 256$	1,085,825	6,514,950	64,843	0.83	2.17
$128 \times 128 \times 512$	8,536,833	51,220,998	160,798	6.49	8.44

Table 5.1: Selected parameter sets for our three base behavior test cases from studies in [1]. Common parameters are  $K_{prob_s} = 550$ ,  $V_{pump} = 2$ , and SR diffusion  $D_s = 0.78$ .

Case	$K_{prob_c}$	SR load ( $s_0$ )	$\hat{\sigma}$
sparking	15	2000	200
wave	10	5000	150
blowup	5	10000	200

different information in relation to the calcium dynamics within the system. CRU plots show the open calcium release units, which are represented by blue dots in the domain. Isosurface plots show the concentration of  $\text{Ca}^{2+}$  in the cytosol. The color blue represents the critical value of  $\text{Ca}^{2+}$  concentration of 65  $\mu\text{M}$ . Higher concentrations on the boundary are indicated by a yellow–red color palette. Line-scans are produced by tracking the concentration of the cytosolic  $\text{Ca}^{2+}$  concentration along the center of the cell at each millisecond. The concentrations of  $\text{Ca}^{2+}$  are plotted on a two-dimensional domain for each second, and then overlayed upon each other producing the final image. Higher concentrations of  $\text{Ca}^{2+}$  are indicated by red, while lower concentrations are indicated by blue. Voltage plots track the average voltage at the center of the cell domain, and then is plotted versus time. SR plots show the concentration of  $\text{Ca}^{2+}$  in the SR as it relates to the right, center, and left of the cell.

In Section 5.1, we present results of one-way coupling between electrical excitation and calcium signaling with an enabled membrane pump. One-way coupling is achieved by only considering the forward connection between the electrical and calcium systems, link ① in Figure 1.1, via non-zero  $\kappa$ . In Section 5.2, we present results of a two-way coupling between the calcium and electrical systems, link ① and link ②. In the two-way coupling, we add in the feedback connection between the electrical and calcium systems. As described in Section 3, two-way coupling is mathematically achieved through the inclusion of a calcium efflux term, scaled by the factor  $\omega$ , referred to as a feedback strength coefficient. We present a parameter study of  $\omega$  in which we examine how varying the value of  $\omega$  impacts the behavior of our solutions.

## 5.1 Electrical Excitation to Calcium Signaling: One-Way Coupling

The first set of simulations run with the parameters set as in Table 5.1 use only the coupling from electrical excitation to calcium signaling. That is,  $\kappa = 0.01$  and  $\omega = 0$ , so that the feedback from calcium signaling to electrical excitation is off. The change here from [1] is the value of  $V_{m_{pump}}$  in (3.15). The pump of calcium leaving the cell was disabled by setting  $V_{m_{pump}} = 0$  in [1], but we introduce the effect of turning on this pump by  $V_{m_{pump}} = 1$ . The resulting behaviors, as observed, are not exactly of the basic three types. These observed behaviors become the base test for our parameter study in  $\omega$  for the effect of turning on the feedback from calcium signaling to electrical excitation.

Section 5.1.1 presents the sparking behavior as before, with more responsiveness to the voltage. In the wave case as shown in Figure 4.1(a) of [1] the linescans show ‘V’ patterns as calcium propagates through the cytosol over time. With  $V_{m_{pump}} = 1$  we see no such action as too much calcium is pumped out of the cell for propagation from calcium-induced calcium release to occur. Instead, we see only a high concentration of calcium sparking around two instances in time, presented in Section 5.1.2. The behavior in Section 5.1.3 is characterized as blowup, but the nature of the blowup is different with  $V_{m_{pump}} = 1$ . Blowup cases were those in which the cell became flooded with calcium and maintained that high concentration of calcium until the final time. In our blowup case we observe the cell floods with calcium, which then leaks out of the cell and another flooding of calcium into the cytosol occurs. This pattern continues a few times over before

the SR calcium store is so depleted that no significant amount of calcium is released into the cell when a CRU opens.

### 5.1.1 Sparking Case

The first behavior we present is sparking. Figure 5.1 shows CRU plots and isosurface plots at a sampling of times over the course of this simulation. At the specific time the CRU plot indicates each open CRU with a single blue dot. The isosurface plot shows the concentration of calcium in the cytosol. In this plot all of the observed concentrations of calcium are very low, so the color is only a blue. Figure 5.2 shows the line scan for this sparking behavior. The scale of this line scan is very sensitive to any release of calcium so that the sparking behavior can be observed, 0–5  $\mu\text{M}$ . The scale will be much less sensitive to low calcium concentrations in the blowup case, 0–100  $\mu\text{M}$ , so that only high levels of calcium are observed. Note there are two places in which more sparking occurs. The voltage plot shows that the spikes in the voltage correspond to these highest times of calcium release, which is a physiologically realistic behavior.

In Figure 5.1 (CRU), the number of CRUs opening increases from 100 ms to 400 ms where at 500 ms the number of open CRUs decreases considerably. This corresponds direction with Figure 5.1 (ISO) where the cytosolic calcium concentration is also at its greatest point in the same timeframe. However the calcium does not “buildup” as is seen at 500 ms by a much lower number open CRUs and a lower concentration of  $\text{Ca}^{2+}$ . The accompanying linescan in Figure 5.2 supports these observations as the cyan color, indicative of heavy sparking, can be seen in the 400 ms region but not in the 500 ms region. The concentration behavior repeats itself from 600 ms to 900 ms in Figure 5.1 (CRU) and Figure 5.1 (ISO). This repetition can also be seen in the linescan in Figure 5.2 during those timeframes.

### 5.1.2 Wave Case

The second behavior observed is extremely heavy sparking, rather than a calcium-induced propagation of a wave through the cell. In fact, we observe what could be considered a very light wave of calcium in the line scan of Figure 5.4.

In Figure 5.3, we see similar behavior as in Figure 5.1, but with higher numbers of open CRUs and higher concentrations of calcium at the corresponding times. We do not see any very high concentrations of calcium, but we readily observe the high number of CRUs open around 400 ms and 900 ms and the higher concentrations of calcium at those times when compared to the sparking case. When looking at the linescan in Figure 5.4, it can be shown that the dark red regions correspond to the heavy

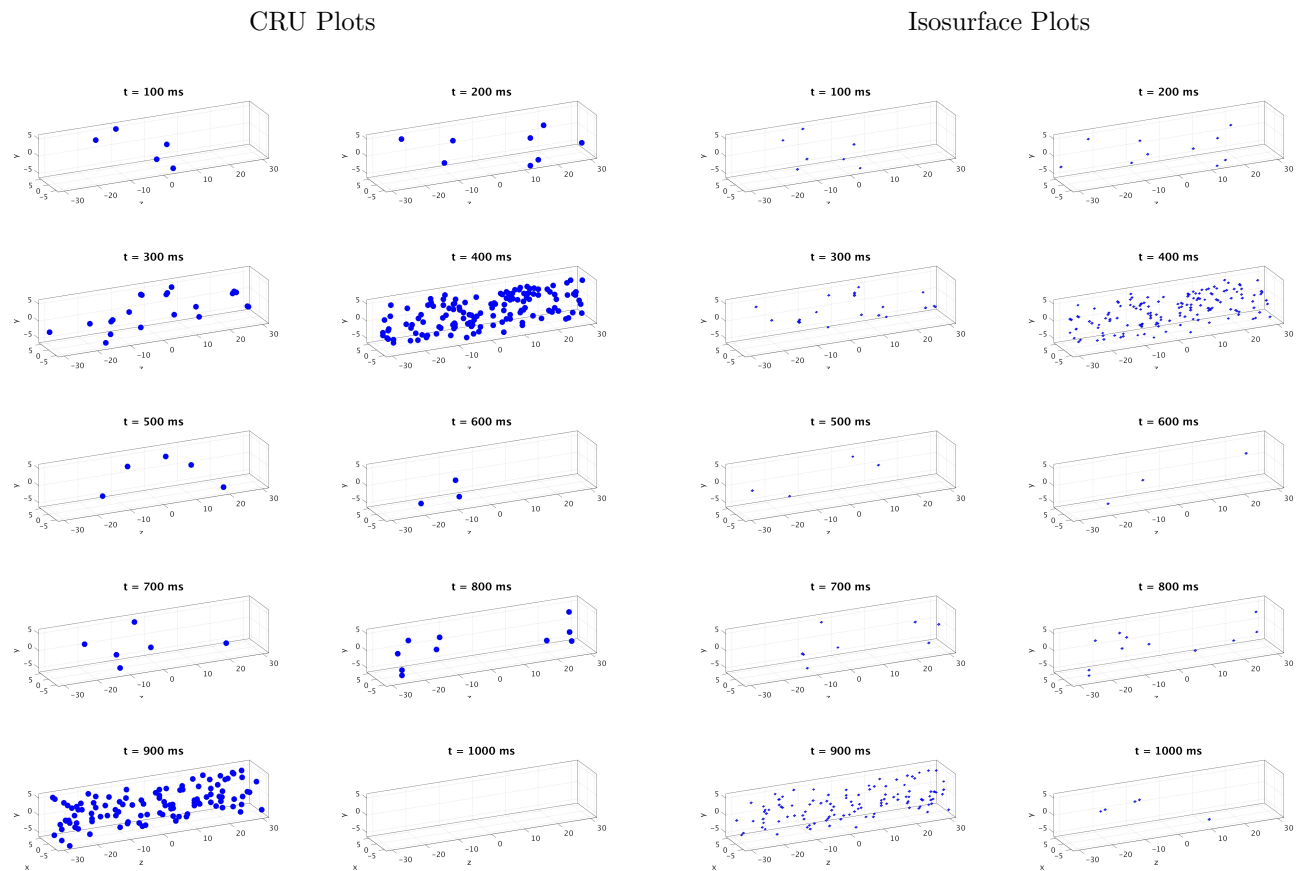
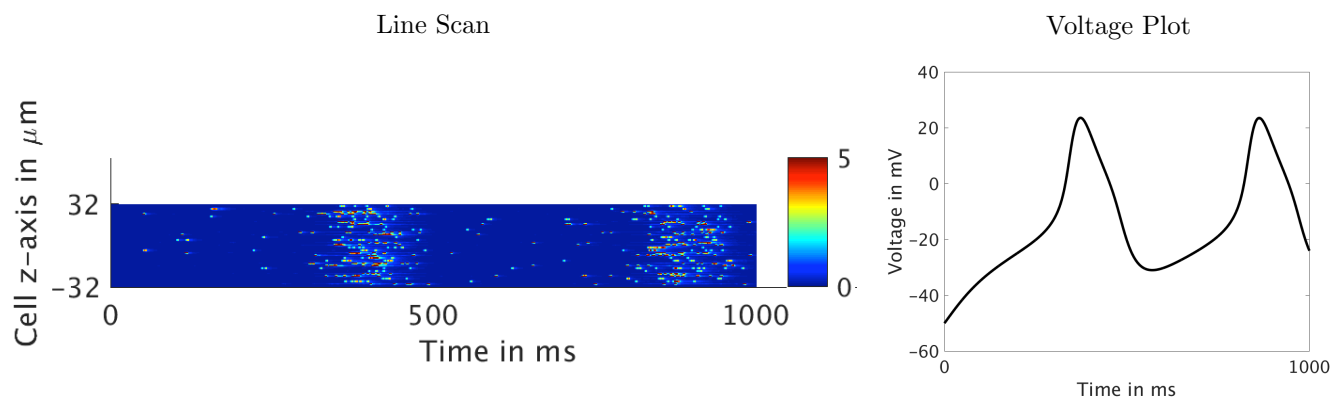
sparking times that can be observed in Figure 5.3 with the ISO and the CRU plots. The scale of this line scan is the same as in the sparking case, very sensitive to any release of calcium so that the behavior can be observed, 0–5  $\mu\text{M}$ . These clearly correspond with the spikes in voltage from the electrical excitation demonstrating a good connection between the systems.

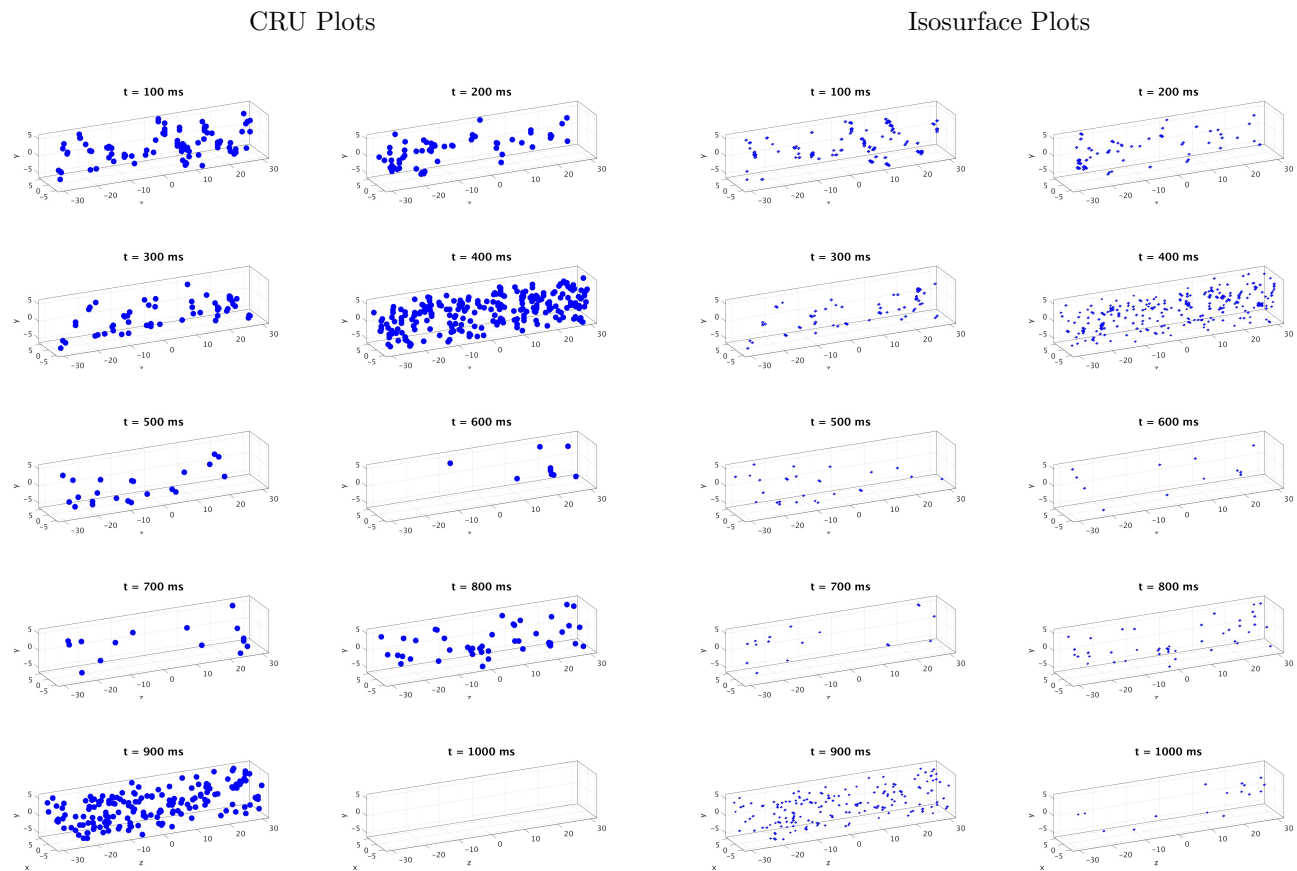
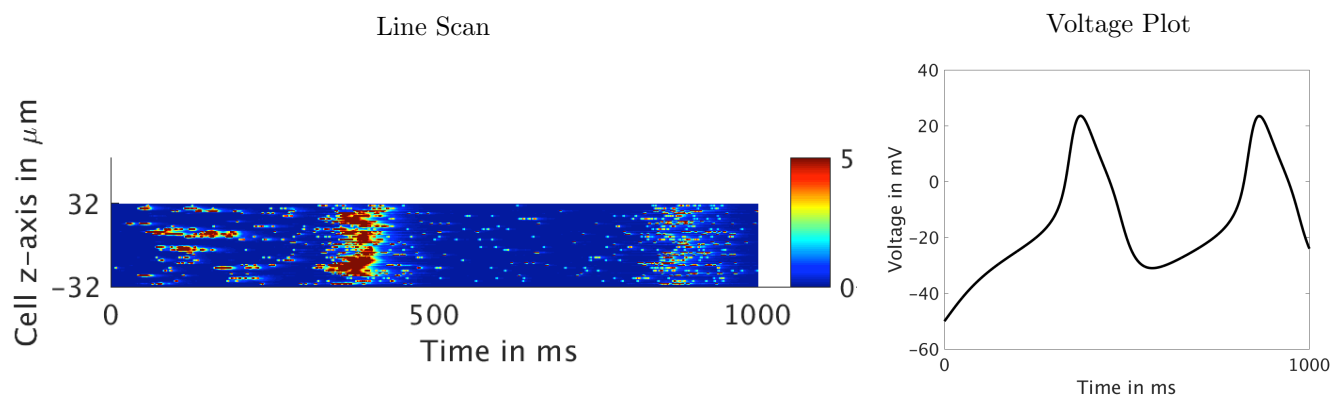
### 5.1.3 Blowup Case

The final case presented here is the blowup case. To reiterate: a blowup case is where the concentration of cytosolic calcium is high early on, at  $t = 50$  ms causing many CRUs to open as seen in Figure 5.5 at  $t = 125$  ms. Then the behavior is repeated in the later images inside Figure 5.5. We consider a high level of calcium to occur when the average cytosolic calcium concentration at some point reaches above 5  $\mu\text{M}$ . The definition of a blowup that was provided does not seem to fit the behavior of this current case. While the concentration of cytosolic calcium is initially, and physiologically, too high it does not however stay high the entire simulation due to the enabling of the membrane pump. Instead the concentration is high for a few milliseconds but goes down to basal levels and then repeats in a periodic fashion. This behavior can be readily seen in the linescan in Figure 5.6, scaled from 0 to 100  $\mu\text{M}$ . It is even improper that, along with high concentrations, the spike in calcium is not in line with a spike in voltage. The voltage should be introducing additional calcium into the system which should only increase the severity of the blowup but there does not appear to be any signs in the linescan that this is happening. The explanation is that the concentration did not stay high for the entire simulation because release of calcium was so severe that the SR was completely depleted of calcium leaving none left to flow into the the cytosol.

## 5.2 Electrical Excitation and Calcium Signaling: Two-Way Coupling

Now that we have demonstrated behaviors in the presence of the one-way coupling from electrical excitation to calcium signaling we consider cases in which two-way coupling is present. We turn on the coupling from calcium signaling to electrical excitation by setting  $\omega > 0$ . For each of the parameter sets that generated the behaviors in Section 5.1 we consider four cases of  $\omega$  to test the feedback strength from calcium signaling and electrical excitation:  $\omega = 10, 30, 50$ , and 100. In this study, we do not change the strength of the connection from electrical excitation to calcium signaling. This is certainly something that would be of interest in future study.

Figure 5.1: CRU plots and isosurface plots for sparking case with  $\omega = 0$ .Figure 5.2: Line scan and voltage plot for sparking case with  $\omega = 0$ .

Figure 5.3: CRU plots and isosurface plots for wave case with  $\omega = 0$ .Figure 5.4: Line scan and voltage plot for the wave case with  $\omega = 0$ .

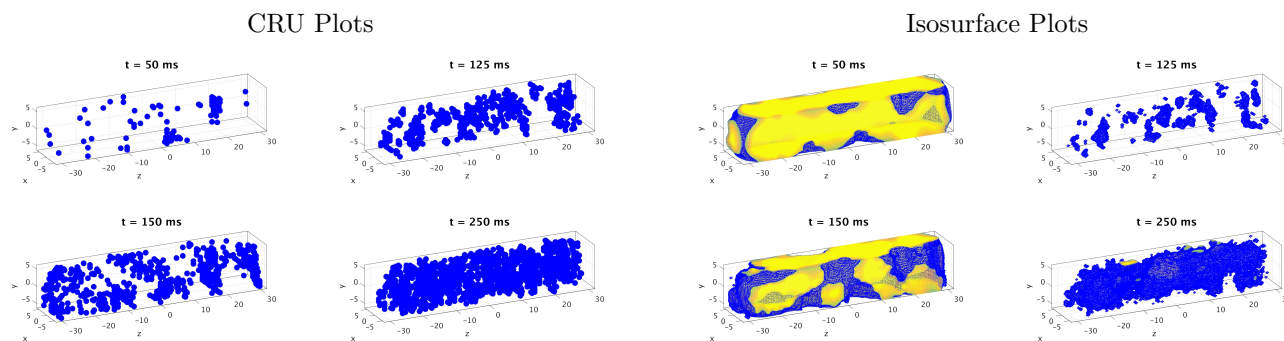


Figure 5.5: CRU plots and isosurface plots for blowup case with  $\omega = 0$ .

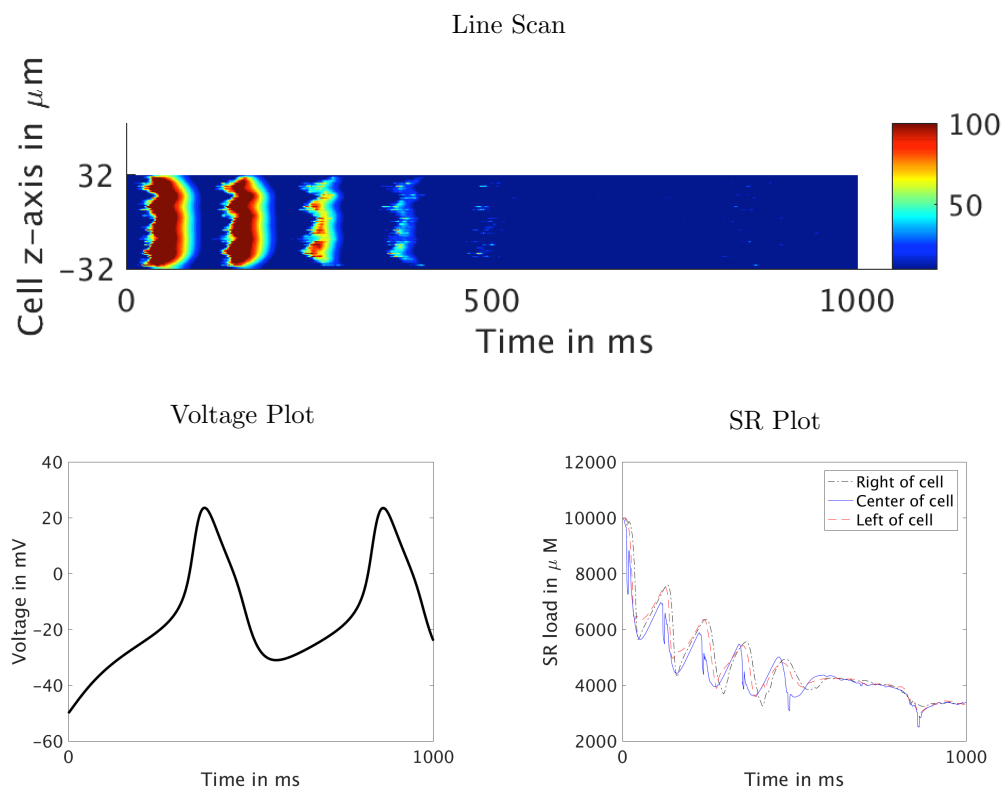


Figure 5.6: Line scan, voltage plot, and SR plot for the blowup case with  $\omega = 0$ .

### 5.2.1 Sparking Case, $\omega > 0$

Under the same parameters as Section 5.1.1, we present simulations with  $\omega = 10$  or 30 in Figure 5.7 and  $\omega = 50$  or 100 in Figure 5.8. We observed that for  $\omega < 10$  the same general behavior as the case  $\omega = 10$  and that of  $\omega = 0$  from Figure 5.2. In the cases in which  $\omega \leq 10$ , we observe that the linescans and voltage plots are synchronized, the two peaks in voltage match up with the heavy concentration of sparking in the line scan around 400 ms and 900 ms. The SR plot of the concentration of calcium ions in the SR also shows the synchronization with this behavior as the SR calcium concentration dips at these times, appropriately, as the release of calcium ions from the SR into the cytosol is exactly the higher concentration of calcium ions in the cytosol we see in the line scan.

For  $\omega = 30$  we present CRU plots and isosurface plots in Figure 5.9. This case is chosen as the voltage plot has a nicer attunement for the changed periodicity in voltage and the linescans for each case look relatively the same with nothing more than a light peppering of color to represent minor sparking.

As we make  $\omega$  larger, we continue to observe differences in the behavior of the average voltage. In particular, for  $\omega = 50$  we observe a third peak in the voltage, which is not matched by a corresponding dip in the SR or by a higher concentration of cytosol calcium sparking shown in the line scan. In this sparking case, we do not see the same depletion over time of the calcium store in the SR as we did with the wave and blowup cases. This indicates there is not a significant amount of calcium ions that are leaving the cell. For that reason, the sparking case is promising as a point of further study. Despite the clear differences in the voltage plots amongst all the  $\omega$  values, the linescans remain more or less unchanged. It should be observed that  $\omega = 50$  having more peaks than  $\omega = 10$  would result in more calcium entering through the excited LCC but this is not observed in the linescans present in Figure 5.7 and Figure 5.8. The easiest idea to deal with is that amount of calcium entering through the LCC is negligible when compared to the amount removed through the  $\omega$  term and pumped into the cytosol by the SR and CRUs.

### 5.2.2 Wave Case, $\omega > 0$

Similar to what happened in Section 5.1.2, the wave case here is also consistently heavy sparking when looking at all the values of  $\omega$ . As expected there are several drastic changes in voltage periodicity as  $\omega$  begins to become much larger like the more natural two peak seen when  $\omega = 10$ , in Figure 5.10, becomes more hectic and less periodic looking when  $\omega = 100$  in Figure 5.11. Unlike in the most recent sparking case,  $\omega$  has a clear impact on

the linescans present in Figure 5.10, and Figure 5.11 particularly when comparing extreme values like  $\omega = 10$  and  $\omega = 100$ . This factor ten increase in  $\omega$  causes a serious amount of heavy sparking to occur throughout the entire linescan of  $\omega = 100$  whereas the linescan for  $\omega = 10$  remains more similar to the wave case where  $\omega = 0$ . For  $\omega = 10$ , the concentration, though less frequent, is much greater when it occurs when compared to linescan of  $\omega = 100$ . The linescans in between demonstrate this metamorphosis in behavior, gradually becoming more frequent but less concentrated.

### 5.2.3 Blowup Case, $\omega > 0$

Under the same parameters as Section 5.1.3, we present simulations with  $\omega = 10$  or 30 in Figure 5.12 and  $\omega = 50$  or 100 in Figure 5.13. While line scans appear similar, there is a clear distinction. As in Section 5.1.3, we experience a repeated blow up. As we increase  $\omega$ , the repeated blowups continue for a longer amount of time. If we examine the accompanying voltage plots, we observe that as  $\omega$  increases, so does the amount of voltage entering the system. Beginning at  $\omega = 50$ , we observe a behavior known as early after-depolarization or EAD. This occurs when an increase of voltage frequency is observed before the previous polarization of influx of voltage is complete. An amalgamation of these behaviors in multiple cardiomyocytes could result in cardiac arrhythmia. SR plots show the amount of  $\text{Ca}^{2+}$  in the SR. We observe that as  $\omega$  increases, the amount of  $\text{Ca}^{2+}$  is being removed (or pumped out) increases.

## 6 Conclusions

We formulated a complete model of the electrical excitation, calcium signaling, and mechanical contraction systems. The calcium and mechanical systems are linked via feedback and feedforward terms for the contractile dynamics model, using the proportion of actin-myosin cross-bridges which are actively linked and therefore generating contractile force at any given time. We introduced a new cytosol species to describe these actin-myosin cross-bridges and introduced a corresponding third cytosol reaction term. We also modified the reaction equation for troponin to more accurately describe the decreased calcium-troponin disassociation rate resulting from the protein's change in shape.

We introduced a calcium dependency into the voltage PDE, controlled by a scaling factor of feedback strength  $\omega$ . The calcium efflux term ( $J_{m_{pump}} - J_{m_{leak}}$ ) represents the only coupling between cytosol calcium levels and voltage in the full set of PDEs, which can be switched on or off by making the feedback strength parameter  $\omega$  a positive value or zeroing it out to sever the



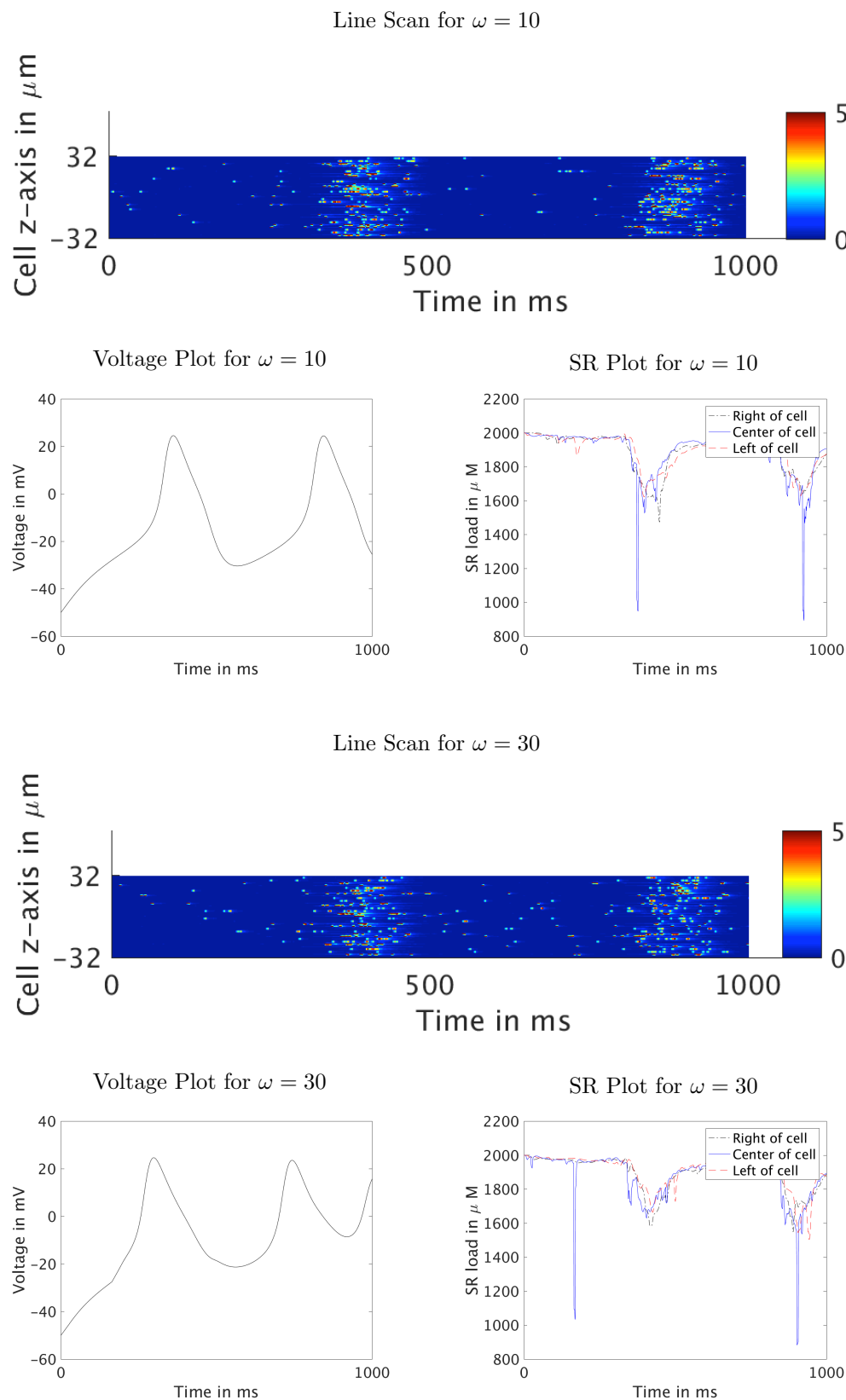
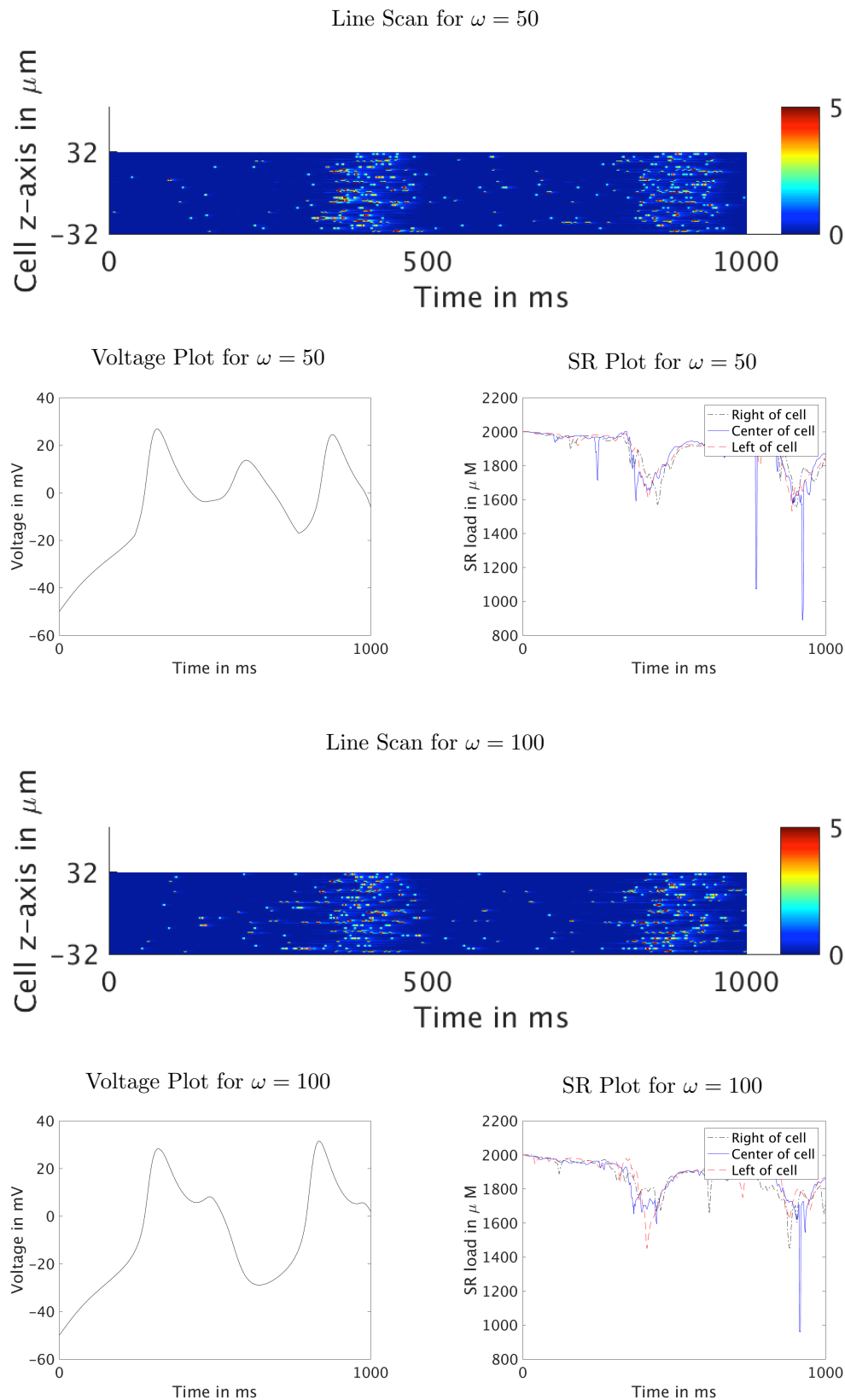


Figure 5.7: Line scans, voltage plots, and SR plots for a spark for  $\omega = 10$  and 30.

Figure 5.8: Line scans, voltage plots, and SR plots for a spark for  $\omega = 50$  and 100.

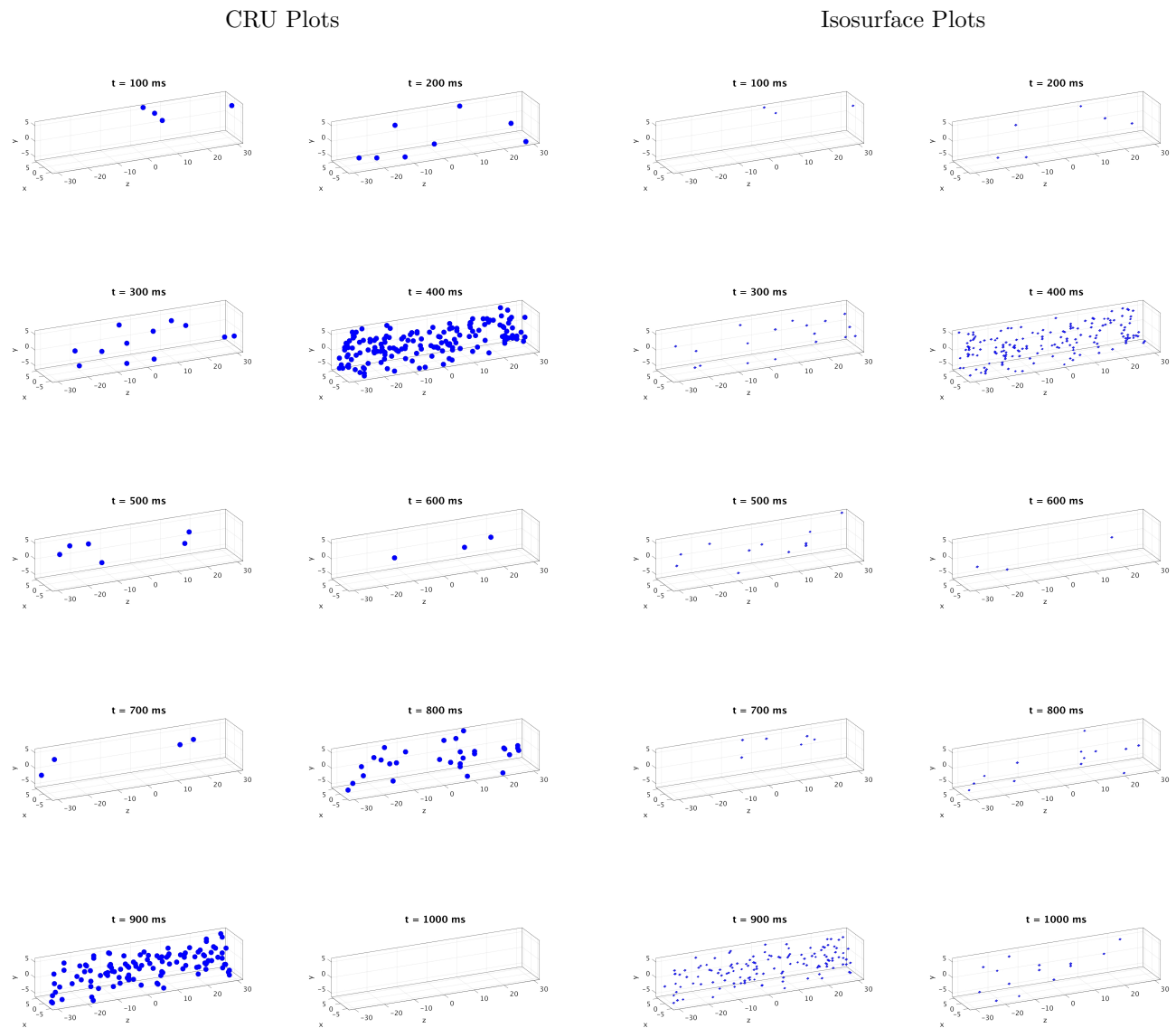


Figure 5.9: CRU plots and isosurface plots for sparking case with  $\omega = 30$ .

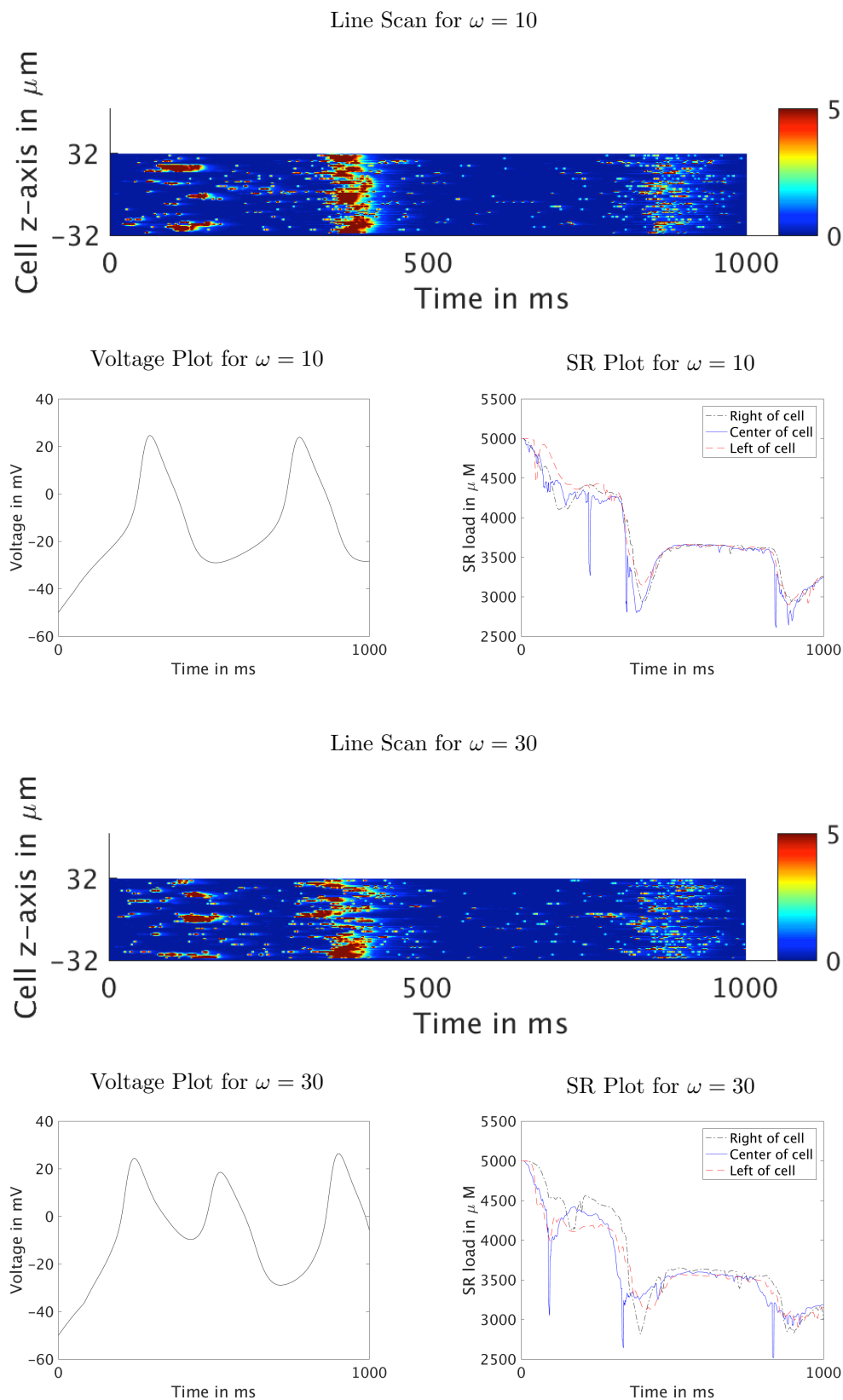
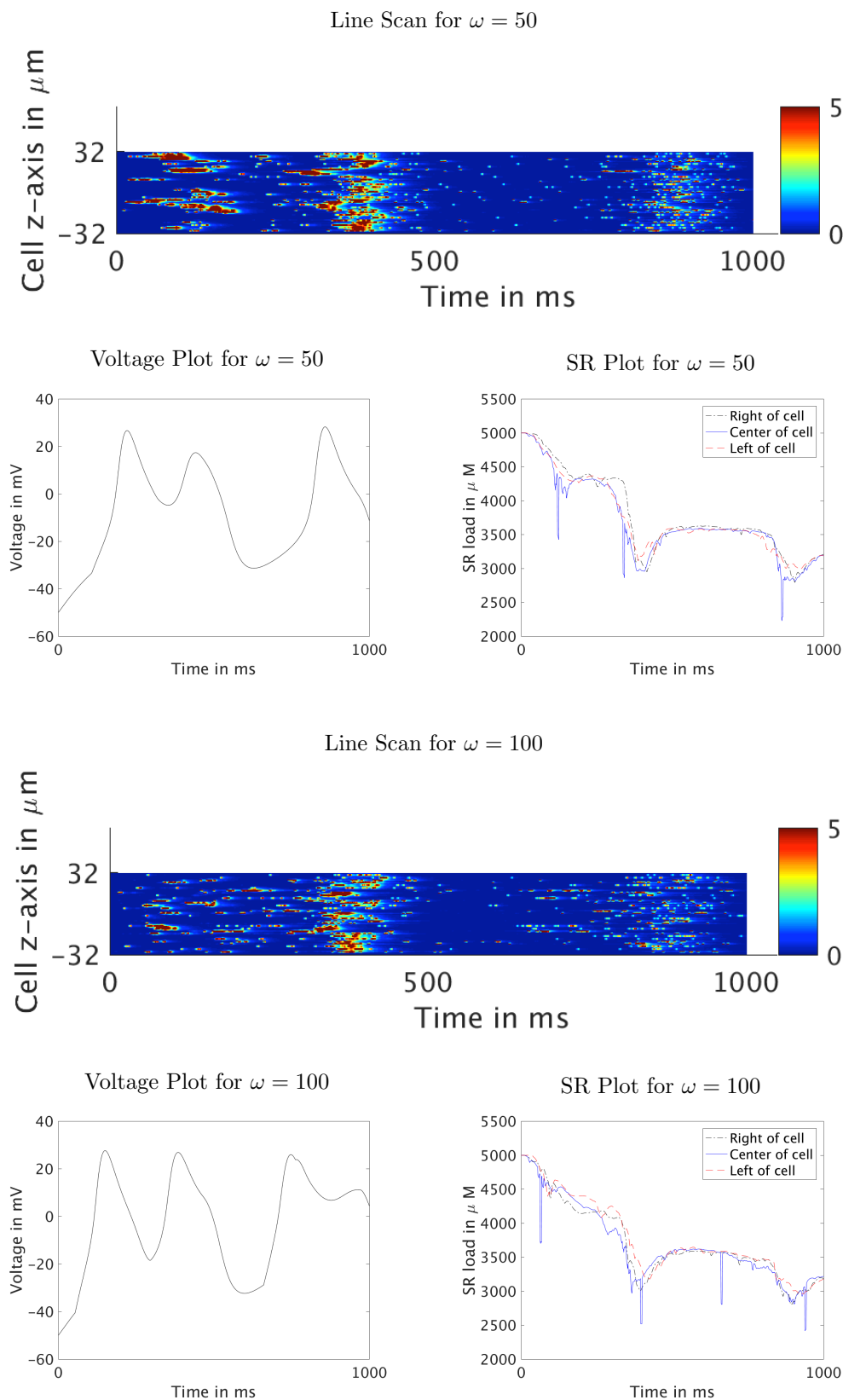
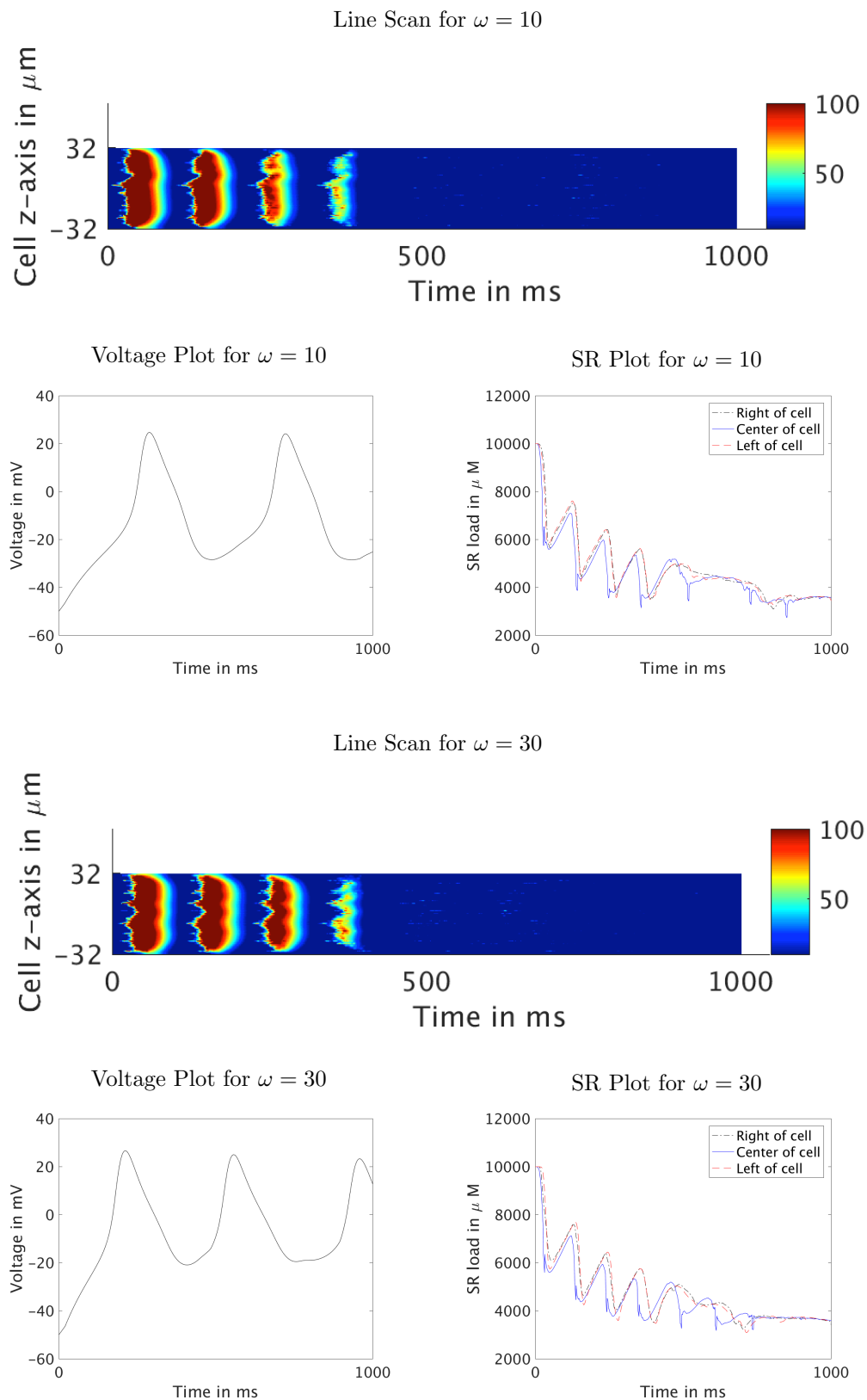
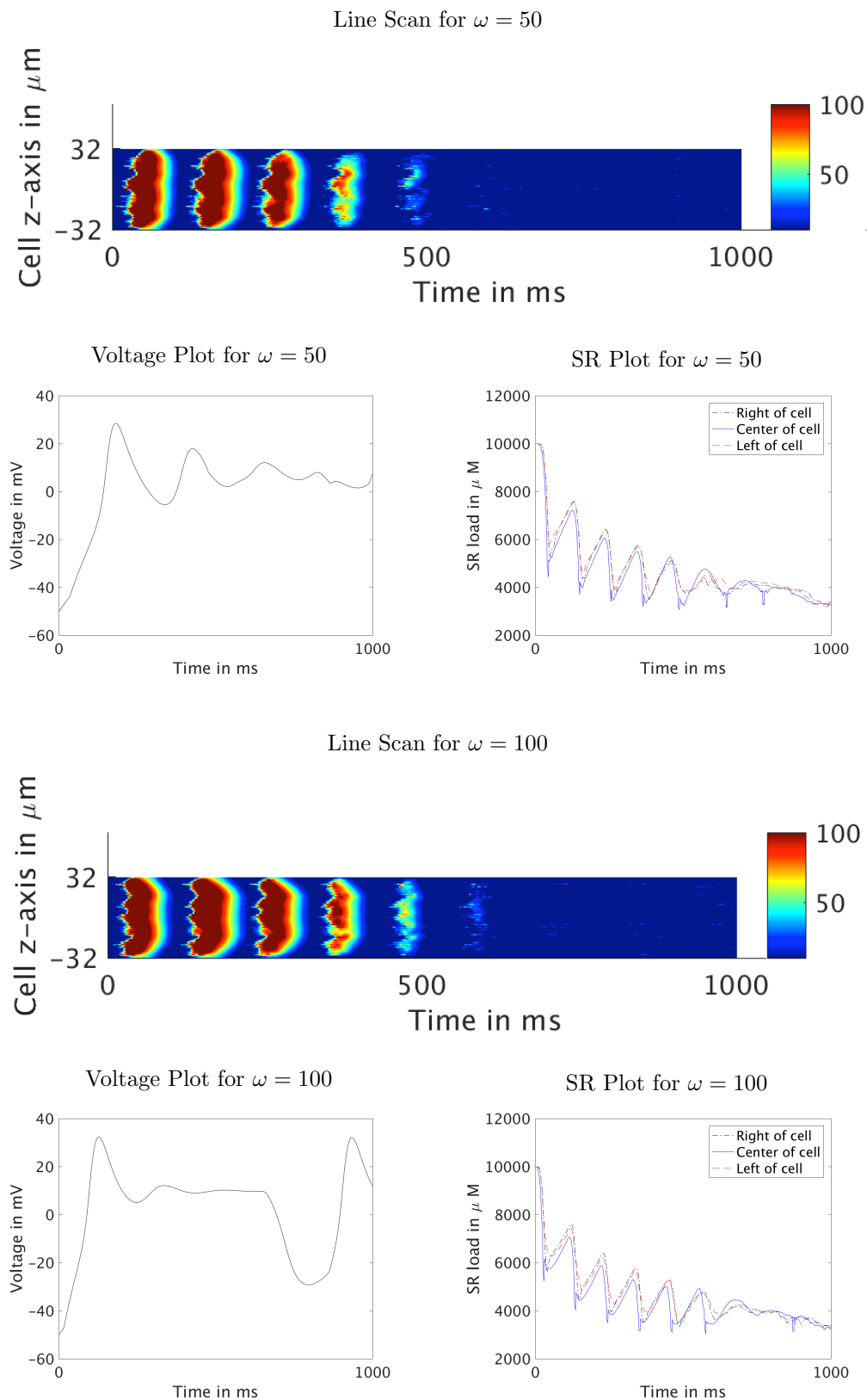


Figure 5.10: Line scans, voltage plots, and SR plots for a wave for  $\omega = 10$  and 30.

Figure 5.11: Line scans, voltage plots, and SR plots for a wave for  $\omega = 50$  and 100.

Figure 5.12: Line scans, voltage plots, and SR plots for blowup for  $\omega = 10$  and 30.

Figure 5.13: Line scans, voltage plots, and SR plots for blowup for  $\omega = 50$  and 100.



connection from the calcium dynamic to the electrical dynamic. Our parameter study indicated that as the coupling strength between the calcium system and the electrical system increases, the duration of the action potential lengthens. The simulated action potential is qualitatively similar to an experimental range and duration. The range of action potential stays between  $-50$  mV and  $+20$  mV, while the duration of the action potential varies. Values for  $\omega$  below 10 are too low to produce notably altered results. However, as we continued to scale  $\omega$  up, we began to see a stronger and stronger influence of the current generated by calcium efflux through the membrane upon the electrical potential of the membrane itself. The formerly steady and unaffected periodicity of the voltage over time first sped up, then deteriorated altogether, as we continued to increase the value. Over strengthening the feedback connection from the current generated by calcium efflux results in physiologically unrealistic behavior.

The formulation of the complete model opens many opportunities for further study. Simulations with 7 species that add the actin-myosin cross-bridges as a third cytosol buffer species thus enabling the feedback and feedforward links from calcium signaling to mechanical contraction. The addition of calsequestrin as a buffer species in the SR is also interesting. Since calsequestrin binds to calcium ions in the SR, it would have impacts across all three systems as less calcium ions would leave the SR. Examining the impact of calsequestrin on all three systems would require the use of 8 species. Less species could be used to examine calsequestrin as it impacts the electrical excitation effects without mechanical effects using 7 species or the calsequestrin impact with mechanical without electrical using only 6 species. We also suggest further study of the membrane pump term is important so that the addition of this term may not have such a significant impact on behaviors. Our introduction of  $\omega$  has enabled a more direct representation of the relationship between cytosol calcium concentration and membrane potential. Thus we are also now able to study the interplay between the strengths of the feedback and feedforward links of electrical excitation and calcium signaling with  $\kappa$  and  $\omega$ .

## Acknowledgments

These results were obtained as part of the REU Site: Interdisciplinary Program in High Performance Computing ([hpreu.umbc.edu](http://hpreu.umbc.edu)) in the Department of Mathematics and Statistics at the University of Maryland, Baltimore County (UMBC), in Summer 2016 [2]. This program is funded by the National Science Foundation (NSF), the National Security Agency (NSA), and the Department of Defense (DOD), with additional support from UMBC,

the Department of Mathematics and Statistics, the Center for Interdisciplinary Research and Consulting (CIRC), and the UMBC High Performance Computing Facility (HPCF). HPCF is supported by the U.S. National Science Foundation through the MRI program (grant nos. CNS-0821258 and CNS-1228778) and the SCREMS program (grant no. DMS-0821311), with additional substantial support from UMBC. Co-author Uchenna Osia was supported in part by the UMBC National Security Agency (NSA) Scholars Program through a contract with the NSA. Graduate assistant Jonathan Graf was supported by UMBC.

## References

- [1] A. M. Alexander, E. K. DeNardo, E. Frazier III, M. McCauley, N. Rojina, Z. Coulibaly, B. E. Peercy, and L. T. Izu. Spontaneous calcium release in cardiac myocytes: Store overload and electrical dynamics. *Spora: A Journal of Biomathematics*, 1(1), 2015.
- [2] K. Angeloff, C. Barajas, A. D. Middleton, U. Osia, J. S. Graf, M. K. Gobbert, and Z. Coulibaly. Modeling the links between the chemical, electrical, and contractile calcium dynamics in a heart cell. Technical Report HPCF-2015-15, UMBC High Performance Computing Facility, University of Maryland, Baltimore County, 2016.
- [3] T. Banyasz, B. Horvath, Z. Jian, L. T. Izu, and Y. Chen-Izu. Profile of l-type  $Ca^{2+}$  current and  $Na^{+}/Ca^{2+}$  exchange current during cardiac action potential in ventricular myocytes. *Heart Rhythm*, 9(1):134–142, 2012.
- [4] Centers for Disease Control and Prevention, National Center for Health Statistics. Number of deaths for leading causes, 2015. <https://www.cdc.gov/nchs/fastats/leading-causes-of-death.htm>, page last updated October 7, 2016; accessed December 22, 2016.
- [5] H. Cheng, W. J. Lederer, and M. B. Cannell. Calcium sparks: elementary events underlying excitation-contraction coupling in heart muscle. *Science*, 262:740–744, 1993.
- [6] J. N. Edwards and L. A. Blatter. Cardiac alternans and intracellular calcium cycling. *Clin. Exp. Pharmacol. P.*, 41(7):524–532, 2014.
- [7] L. E. Ford and R. J. Podolsky. Regenerative calcium release within muscle cells. *Science*, 167:58–59, 1970.

- [8] S. A. Gaeta, T. Krogh-Madsen, and D. J. Christini. Feedback-control induced pattern formation in cardiac myocytes: a mathematical modeling study. *J. Theor. Biol.*, 266(3):408–418, 2010.
- [9] M. K. Gobbert. Long-time simulations on high resolution meshes to model calcium waves in a heart cell. *SIAM J. Sci. Comput.*, 30(6):2922–2947, 2008.
- [10] A. L. Hanhart, M. K. Gobbert, and L. T. Izu. A memory-efficient finite element method for systems of reaction-diffusion equations with non-smooth forcing. *J. Comput. Appl. Math.*, 169(2):431–458, 2004.
- [11] X. Huang, M. K. Gobbert, B. E. Peercy, S. Kopecz, P. Birken, and A. Meister. Order investigation of scalable memory-efficient finite volume methods for parabolic advection-diffusion-reaction equations with point sources. In preparation (2016).
- [12] L. T. Izu, J. R. H. Mauban, C. W. Balke, and W. G. Wier. Large currents generate cardiac  $\text{Ca}^{2+}$  sparks. *Biophys. J.*, 80:88–102, 2001.
- [13] L. T. Izu, S. A. Means, J. N. Shadid, Y. Chen-Izu, and C. W. Balke. Interplay of ryanodine receptor distribution and calcium dynamics. *Biophys. J.*, 91:95–112, 2006.
- [14] L. T. Izu, W. G. Wier, and C. W. Balke. Evolution of cardiac calcium waves from stochastic calcium sparks. *Biophys. J.*, 80:103–120, 2001.
- [15] C. Morris and H. Lecar. Voltage oscillations in the barnacle giant muscle fiber. *Biophys. J.*, 35(1):193, 1981.
- [16] P. S. Pacheco. *Parallel Programming with MPI*. Morgan Kaufmann, 1997.
- [17] Z. Qu, M. Nivala, and J. N. Weiss. Calcium alternans in cardiac myocytes: Order from disorder. *J. Mol. Cell. Cardiol.*, 58:100–109, 2013.
- [18] J. Sanderson. The SWORD of Damocles. *Lancet*, 348(9019):2–3, 1996.
- [19] J. Schäfer, X. Huang, S. Kopecz, P. Birken, M. K. Gobbert, and A. Meister. A memory-efficient finite volume method for advection-diffusion-reaction systems with non-smooth sources. *Numer. Methods Partial Differential Equations*, 31(1):143–167, 2015.
- [20] T. I. Seidman, M. K. Gobbert, D. W. Trott, and M. Kružík. Finite element approximation for time-dependent diffusion with measure-valued source. *Numer. Math.*, 122(4):709–723, 2012.
- [21] S. Wagner, L. S. Maier, and D. M. Bers. Role of sodium and calcium dysregulation in tachyarrhythmias in sudden cardiac death. *Circ. Res.*, 116(12):1956–1970, 2015.
- [22] J. N. Weiss, A. Garfinkel, H. S. Karagueuzian, P. S. Chen, and Q. Zhilin. Early afterdepolarizations and cardiac arrhythmias. *Heart Rhythm*, 7(12):1891–1899, 2010.